Impact of lightning NO emissions on North American photochemistry as determined using the Global Modeling Initiative (GMI) model

Dale Allen,[1] Kenneth Pickering,[2] Bryan Duncan,[2] and Megan Damon[3,4]

Received 2 March 2010; revised 11 June 2010; accepted 18 June 2010; published 19 November 2010.

[1] The impact of nitric oxide (NO) emissions by lightning on summertime North American nitrogen oxides (NO_x) and ozone is studied using the Global Modeling Initiative (GMI) CTM and an improved lightning NO algorithm. The spatial distributions of modeled and National Lightning Detection Network-based flash rates during the summers of 2004–2006 agree well (R^2 = 0.49, 18% low bias). Despite this reasonable agreement, 9–12 km model NO_x during the Intercontinental Chemical Transport Experiment (INTEX-A) campaign is a factor of 2.2–3.6 too low for a simulation that includes a 480 mol per flash midlatitude lightning NO source, the source that provides the best agreement with measurements. Possible causes of this low bias include biases in model convection and/or too rapid NO_x chemistry in the upper troposphere. Model tropospheric NO_2 columns over the southeastern United States during these summers show a 7% high bias with respect to the OMI DOMINO/GEOS-Chem tropospheric column NO_2 product. Observed changes between 2004 and 2006 in upper tropospheric ozone at southeastern U. S. INTEX Ozonesonde Network Study sites are captured by the model and appear to be caused by a stronger upper tropospheric anticyclone in 2006 that led to an increase from 21 to 30 ppbv between 2004 and 2006 in the amount of ozone with a lightning NO source; lightning NO emissions were 15%–20% larger in 2004. The contribution of lightning NO to monthly average summertime 300 hPa NO_x over the eastern United States during 2004–2006 varies from 61%–73% (0.09–0.16 ppbv), while the contribution to ozone varies from 19%–31% (15–24 ppbv).

Citation: Allen, D., K. Pickering, B. Duncan, and M. Damon (2010), Impact of lightning NO emissions on North American photochemistry as determined using the Global Modeling Initiative (GMI) model, *J. Geophys. Res.*, *115*, D22301, doi:10.1029/2010JD014062.

1. Introduction

[2] Tropospheric ozone is an important atmospheric pollutant and greenhouse gas whose precursors include reactive odd nitrogen (NO_x) and volatile organic compounds (VOCs). Atmospheric sources of NO_x include fossil fuel emissions (28–32 Tg N/yr), biomass burning emissions (4–24 Tg N/yr), soil microbial emissions (4–16 Tg N/yr), stratospheric decomposition of nitrous oxide (N_2O) (0.1–1 Tg N/yr), aircraft emissions (0.7–1 Tg N/yr), and lightning NO emissions (2–8 Tg N/yr), where estimates of source magnitudes are taken from *Schumann and Huntrieser* [2007] and sources therein.

[3] Production of NO by lightning (LNO_x) is a particularly important NO_x source in the tropics throughout the year and in the midlatitudes, especially over the United States during the summertime [e.g., *Biazar and McNider*, 1995; *Lamarque et al.*, 1996; *Berntsen and Isaksen*, 1999; *Levy et al.*, 1999; *Tie et al.*, 2001; *Hauglustaine et al.*, 2001; *Bond et al.*, 2001, 2002; *Grewe et al.*, 2001; *Zhang et al.*, 2003]. For example, model simulations by *Grewe* [2007] show that up to 70% of total reactive odd nitrogen (NO_y) in the tropical upper troposphere is from lightning with much of it existing in the form of nitric acid (HNO_3) and peroxyacetylnitrate (PAN).

[4] In most of the free troposphere ozone production rates are highly sensitive to NO_x mixing ratios. Therefore mid- and upper-tropospheric ozone concentrations are substantially enhanced by lightning NO emissions. For example, *Hauglustaine et al.* [2001] used the Model of Ozone and Related Tracers (MOZART) to determine the enhancement of ozone associated with LNO_x. They found that LNO_x was responsible for a 150% increase in 250 hPa summertime ozone over South America and Africa and a greater than 100% increase over the South Atlantic. In the Northern

[1]University of Maryland College Park, College Park, Maryland, USA.
[2]Code 613.3, NASA-GSFC, Greenbelt, Maryland, USA.
[3]Northrop Grumman Information Technology, Greenbelt, Maryland, USA.
[4]Software Integration and Visualization Office, NASA-GSFC, Greenbelt, Maryland, USA.

Copyright 2010 by the American Geophysical Union.
0148-0227/10/2010JD014062

Hemisphere summer, ozone at 250 hPa increased by 120% over South Asia and 20%–50% over North America and Europe.

[5] *Li et al.* [2005] used GEOS-Chem to study the summertime outflow of North American pollution to the Atlantic. They found that convective outflow over the eastern United States is often trapped within a semipermanent upper troposphere anticyclone centered over the southern United States [see also *Cooper et al.*, 2007, 2009]. Rapid ozone production occurs within this anticyclone as lofted ozone precursors with anthropogenic and biogenic sources are mixed with free troposphere lightning NO emissions. The rapid ozone production and recirculation contributes to an ozone maximum (>80 ppbv) over the southern United States. *Zhang et al.* [2003] used MOZART to investigate the enhancement of ozone associated with lightning NO emissions in this region. They found that lightning NO emissions increased mid and upper tropospheric NO_x amounts by 60%–90% and mid and upper tropospheric ozone amounts by 20%–30%. Measurements taken during the 2004 International Consortium for Atmospheric Research on Transport and Transformation (ICARTT) experiment allowed the summertime NO_x and ozone budgets over the United States to be examined in more detail. Analyses of the ICARTT period by *Cooper et al.* [2006], *Bertram et al.* [2007], and *Hudman et al.* [2007] confirmed the important role lightning NO plays in determining the summertime ozone budget over North America.

[6] *Cooper et al.* [2007] used version 5 of the atmospheric general circulation model European Center Hamburg Modular Earth Submodel System (ECHAM-5 MESSy) [*Jöckel et al.*, 2006] to isolate the contribution of LNO_x to the summertime ozone maximum in August 2006. They determined that LNO_x was responsible for the production of 25–30 ppbv of ozone at 250 hPa over the southern United States and that more than 80% (70%) of summertime upper tropospheric NO_x (ozone) has a probable lightning source. *Cooper et al.*'s estimate was for a month during which atmospheric conditions were particularly conducive for ozone formation. *Choi et al.* [2008] found a smaller enhancement for July–August 2005 in a simulation with the Regional Chemical Transport Model (REAM). They found that lightning NO emissions contributed 15–20+ ppbv to 325 hPa ozone over the southeastern United States and western Atlantic. *Pfister et al.* [2008] used version 4 of MOZART as a tool to study the budget of ozone during the Intercontinental Chemical Transport Experiment (INTEX-A) period. They found that lightning contributed 10% ± 2% to the tropospheric ozone column at INTEX Ozonesonde Network Study (IONS) sites during the INTEX-A time period. *Hudman et al.* [2009] found a 10–17 ppbv enhancement of ozone due to lightning NO emissions extending from the southern United States/Gulf of Mexico region downwind across the subtropical Atlantic toward Europe.

[7] In this study, an improved lightning NO algorithm for the NASA Global Modeling Initiative (GMI) CTM [*Duncan et al.*, 2007, 2008; *Considine et al.*, 2008] is introduced. An improved lightning algorithm was developed because the existing algorithm used monthly average lightning NO emissions constrained by climatological ISCCP cloud top heights [*Price and Rind*, 1992; *Price et al.*, 1997]. This monthly average approach was not appropriate because emissions did not necessarily occur at the same locations as model convection. The enhanced GMI model is used along with ozonesonde, aircraft, and satellite observations to evaluate the impact of lightning NO emissions on North American NO_x and ozone distributions during the summers of 2004–2006.

2. GMI Modeling System

[8] The GMI CTM is designed to be an assessment tool and a component of the NASA Goddard Chemistry and Climate Model (NASA-CCM) [*Pawson et al.*, 2008].

2.1. GMI Chemical Package

[9] The GMI model includes a combined stratosphere-troposphere chemical mechanism with 124 species, 322 chemical reactions, and 81 photolysis processes. The tropospheric portion of the chemical mechanism includes a detailed description of tropospheric ozone, NO_x, and hydrocarbon photochemistry [*Bey et al.*, 2001]. It has been updated with recent experimental data from *Tyndall et al.* [2001] and *Atkinson and Arey* [2003] and data for the quenching reactions of $O(^1D)$ by N_2, O_2, and H_2O [*Ravishankara et al.*, 2002; *Dunlea and Ravishankara*, 2004]. It is integrated using the SMVGEAR II algorithm [*Jacobson*, 1995]. Photolysis rates in the troposphere and stratosphere are calculated using the Fast-JX radiative transfer algorithm [*Wild et al.*, 2000; *Bian and Prather*, 2002], an efficient algorithm that calculates photolysis rates in the presence of an arbitrary mix of cloud and aerosol layers. The scheme treats both Rayleigh scattering as well as Mie scattering by clouds and aerosol. Radiative and heterogeneous effects of aerosols on photochemistry are included. Biogenic emissions of isoprene and monoterpenes are calculated online as in the work of *Guenther et al.* [2006]. Time-appropriate biomass burning emissions are used from the GFEDv2 emission inventory [*van der Werf et al.*, 2006].

[10] The GMI-CTM simulates the radiative and heterogeneous chemical effects of sulfate, dust, sea salt, organic carbon, and black carbon aerosol on tropospheric photochemistry. Three-dimensional aerosol surface area distributions are calculated offline using a 2001 simulation of the Goddard Chemistry Aerosol Radiation and Transport (GOCART) model [*Chin et al.*, 2002] that takes into account swelling of aerosols in humid environments. The emission rates for sea salt, sulfate, black carbon (BC), organic carbon (OC), and dust are monthly averages. The annual emissions are given in Table 1 of *Chin et al.* [2002]. The aerosol fields were coupled to the trace gas distributions as described by *Martin et al.* [2003]. One important modification to this implementation is that the reaction probability for N_2O_5 is now a function of aerosol type, relative humidity, and temperature and is significantly lower than earlier estimates [*Evans and Jacob*, 2005].

[11] Globally, annual anthropogenic (sum of fossil fuel and biofuel) emissions of NO and CO in the GMI CTM equaled 27.4 Tg N and 537 Tg CO, respectively, during each year of the simulation. Biomass burning emissions were year specific. Global biomass burning emissions of CO equaled 431, 428, and 414 Tg CO for 2004–2006, respec-

Table 1. Bias (ppbv) Between Modeled and Measured Upper Tropospheric Ozone During the Summers of 2004 and 2006 at Wallops Island, VA; Houston, TX; and Huntsville, AL IONS Sites

	No Lightning		Low NO_x		High NO_x	
Simulation	2004	2006	2004	2006	2004	2006
IONS Site						
Wallops	−19	−24	−4	−5	+3	+3
Houston	−28	−35	−14	−11	−8	−2
Huntsville	−24	−35	−9	−14	−2	−6

tively. Global biomass burning emissions of NO equaled 5.3, 5.3, and 5.0 Tg N over this time period. Anthropogenic emissions of NO_x over the United States were originally based on the EPA 1999 National Emissions Inventory (NEI99). However, for this 2004–2006 simulation, June to September emissions of NO were reduced by 22% with respect to NEI99 over the United States to account for reductions in power plant emissions associated with the NO_x State Implementation Plan Call [*Hudman et al.*, 2007; *Frost et al.*, 2006]. Power plant emissions of NO_x over the eastern United States during the ozone season decreased by 43% between 1995–2002 and 2003–2006 [*Bloomer et al.*, 2009]. Model anthropogenic emissions of NO_x amount to 0.67 Tg N over the contiguous United States (130°W–70°W, 25°N–50°N) during the INTEX-A period (1 July to 15 August), a period of focus during this study. This emission source is slightly higher than the 0.62 Tg N source used in GEOS-Chem for simulations of this same time period [*Hudman et al.*, 2007]. Globally anthropogenic NO_x emissions during this period equal 3.3 Tg N. Anthropogenic emissions of CO during the same time period equaled 11.2 and 63.4 Tg CO for the contiguous United States and the globe, respectively. Biomass burning emissions over the contiguous United States were only a minor source of CO and NO_x.

2.2. Transport Core and Driving Meteorological Fields

[12] The GMI-CTM can be driven by meteorological fields from version 4 [*Bloom et al.*, 2005] or version 5 [*Rienecker et al.*, 2008] of the NASA-Goddard Earth Observing System (GEOS) General Circulation Model (GCM) and Data Assimilation System (DAS). The simulations presented here were driven by the GEOS-4 DAS. The GEOS-4 GCM was jointly developed by the Global Modeling and Assimilation Office (GMAO) at NASA Goddard and the Climate and Global Dynamics Division at National Center for Atmospheric Research (NCAR). *Lin* [2004] describes the finite volume dynamical core. Physics parameterizations were adopted from version 3 of the NCAR CCM and the Whole Atmosphere Community Climate Model (WACCM) [*Kiehl et al.*, 1985; 1998]. *Zhang and McFarlane* [1995] describe the method used to parameterize deep convection. *Bloom et al.* [2005] provide details on the GEOS-4 GCM and also describe modifications and enhancements to CCM3 physics that were made while constructing the GEOS-4 GCM and DAS. The vertical structure of the GEOS-4 output is a generalized hybrid sigma-pressure coordinate system that includes 42 layers and a smooth transition between sigma in the troposphere (representative pressures > 176 hPa) and pressure in the stratosphere. The model top is at 0.01 hPa. Before use in the GMI CTM, 1° in latitude × 1.25° in longitude output was degraded to 2° × 2.5°.

2.3. Lightning NO Emissions

[13] Global CTMs require the lightning NO source as a function of time and space. The source strength depends on the flash frequency, flash energy, and the NO production per unit energy. Our understanding of the geographical distribution of the flash frequency has increased greatly during the last decade as satellite flash count information has become available from the Optical Transient Detector (OTD) [*Boccippio et al.*, 2000; *Christian et al.*, 2003] and the Lightning Imaging Sensor (LIS) [*Boccippio et al.*, 2002; *Mach et al.*, 2007]. It might seem reasonable to directly use observed flashes when specifying flash frequency in CTMs; however, lightning production is highly correlated with upward vertical motion. In addition, the upper tropospheric concentrations of other ozone precursors with low-level sources, such as odd hydrogen (HO_x) and its precursors (e.g., peroxides, acetone, water vapor, etc.) are likely to be enhanced in regions of upward motion. Therefore, it is necessary to parameterize the flash rate in terms of model fields, such that the lightning occurs at the same times and locations as the vertical transport of ozone precursors. Satellite-retrieved flash rates are useful for constraining flash frequencies obtained using theoretical and/or empirical relationships between model convective fields (e.g., cloud top height, convective mass flux, convective precipitation rate, convective available potential energy) and observed flash rates.

[14] Early versions of the GMI model parameterized flash rates in terms of climatological monthly average ISCCP cloud top heights [*Price and Rind*, 1992; *Price et al.*, 1997]. This algorithm has been replaced by a new scheme that is similar to the method of *Allen and Pickering* [2002] in that it uses upward cloud mass flux in the upper troposphere as the indicator of when and where lightning NO emissions occur. The 2002 scheme used upward cloud mass flux as the predictor variable for lightning flash rate through best fit polynomials developed from ranked distributions of this variable and observed National Lightning Detection Network (NLDN) [*Cummins et al.*, 1998; *Orville and Huffines*, 2001] flash rates. The new scheme assumes flash rates are proportional to the square of upward convective mass flux but then constrains flash rates on an individual grid cell basis to ensure that flash rates when averaged over a period of interest match monthly average climatological flash rates from v2.2 of the OTD/LIS climatology. Details on this lightning NO emission algorithm follow.

[15] The calculation of lightning NO emissions in the GMI CTM is a two step procedure. In step 1, the lightning flash frequency is calculated for each model grid point and the resulting lightning NO_x production rate is determined for each model column. In step 2, the resulting emissions are partitioned in the vertical.

[16] The flash frequency ($LF_{i,j}$) for grid box (i,j) is obtained by multiplying global (G) and local ($\alpha_{i,j}$) scaling factors by the upper tropospheric deep convective mass flux to the power γ. Mathematically,

$$LF_{i,j} = G \times \alpha_{i,j} \times \left(\mathrm{zmmu}_{i,j} - \mathrm{threshold}\right)^{\gamma}, \qquad (1)$$

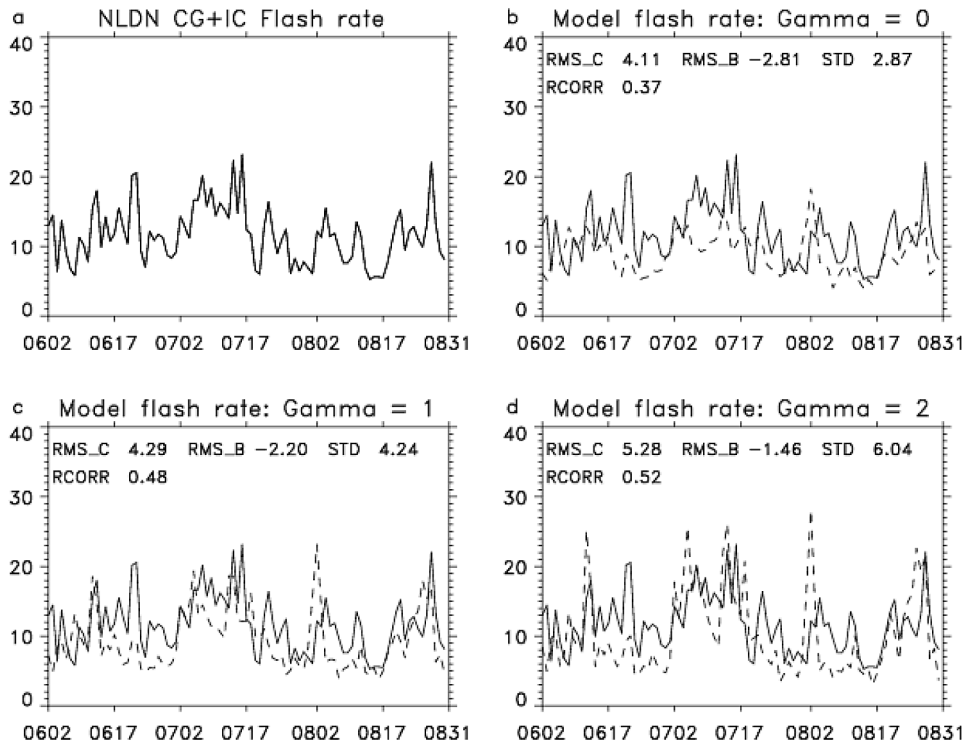

Figure 1. Time series compared NLDN-based total flash rates (a) over the United States during the summer of 2004 with model flash rates for (b) $\gamma = 0$, (c) $\gamma = 1$, and (d) $\gamma = 2$.

where "zmmu" is the deep convective mass flux at GEOS-4 GCM sigma layer 9 (~434 hPa), "threshold" is the value of zmmu below which the flash rate is assumed to equal zero, and γ is a power (0, 1, or 2). The choice of sigma layer 9 limits lightning production by this parameterization to clouds with clouds tops of <~440 hPa (i.e., deep convective clouds). This definition of deep convection is consistent with the definition used by the International Satellite Cloud Climatology Project (ISCCP) [*Rossow et al.*, 1996] and is used in the work of *Allen and Pickering* [2002]. The value chosen for γ determines the amount of weighting assigned to the magnitude of zmmu when calculating the flash rates. For $\gamma = 0$, the magnitude of zmmu gives little or no (for *threshold* = 0) information on the flash rate intensity associated with each deep convective event. As γ increases, the magnitude of zmmu plays an increasingly important role in determining the flash rate associated with each event. Increasing the value of *threshold* decreases the spatial coverage of lightning but increases the intensity of lightning-producing events, while decreasing the value of *threshold* does the opposite. In theory, *threshold* can be chosen so that the time-averaged spatial coverage of model-calculated flashes matches the time-averaged spatial coverage of observed flashes from a detection network such as the NLDN. In this study, we set *threshold* equal to 0.57 kg m^{-2} min^{-1}. For this value of *threshold*, when averaged over 2001, lightning flashes occur in 6.6% of GEOS-4 DAS grid boxes. The deep convective mass flux (zmmu) exceeds zero in 19.9% of grid boxes during the same time period. Figure 1 compares model flash rate time series ($\gamma = 0$, $\gamma = 1$, and $\gamma = 2$) over the eastern United States (110°W–70°W, 25°N–45°N) during the summer of 2004 with NLDN-based CG + IC flash rates during the same period. NLDN-based total flash rates were calculated by aggregating CG flashes from the NLDN onto the 2° × 2.5° GMI grid and then multiplying the resulting flash rates by $Z + 1$, where Z is the climatological IC to CG ratio appropriate for that grid box and month. *Boccippio et al.* [2001] provide values for Z on a 0.5° × 0.5° grid. These values were smoothed with a 7.5° east-west and north-south filter before mapping onto the GMI grid. *Boccippio et al.*'s IC/CG ratios were originally obtained using colocated NLDN and OTD flashes over the United States during the May 1995 to April 1999 time period. The mean Z during this time period was 2.94. Most detected NLDN flashes are CG in character although a recent upgrade in the NLDN network has made it possible to record a small percentage of IC flashes. In this study, NLDN flashes with peak currents (I_p) between 0 and 20 kA are assumed to be IC in character [*Biagi et al.*, 2007] and were removed from the database. Resulting NLDN-based flash rates were then divided by the detection efficiency, where the detection efficiency was obtained from the Vaisala detection efficiency model (Ron Holle, personal communication, 2010) but constrained to be between 0.1 and 0.93, where 0.93 is the estimated detection efficiency of the NLDN over the United States during the 2004–2006 time period [*Biagi et al.*, 2007].

[17] Globally, increasing γ leads to an increase in flash rates over midlatitudes and a decrease in flash rates over the tropics. Over the eastern United States, the increase in flash rates as γ increases from 0 to 2 reduces the centered root mean square bias (rms_b) between modeled and observed flash rates from −2.8 to −1.5 flashes s^{-1}. Increasing γ from 0 to 2 doubles day-to-day variability (σ increases from 2.9 to

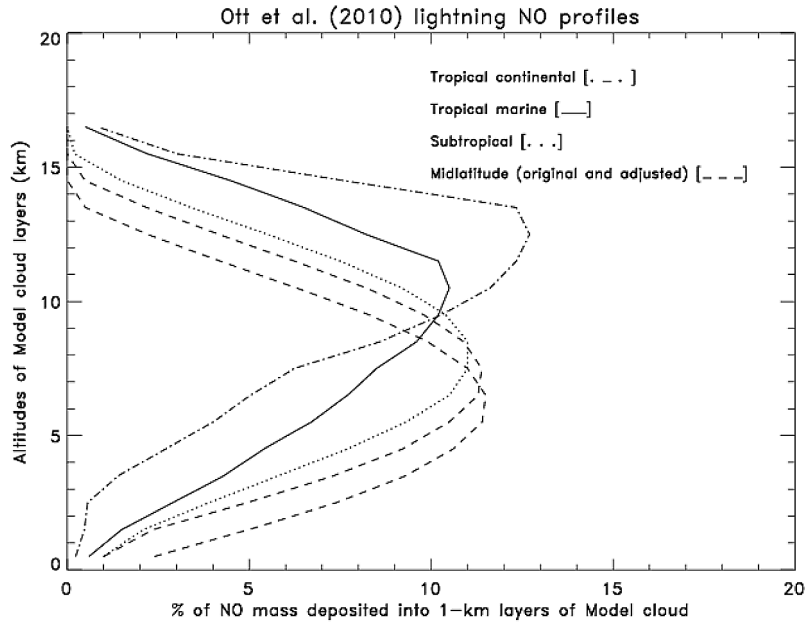

Figure 2. Vertical profile showing lightning NO emissions from *Ott et al.* [2010] as a function of altitude for tropical marine locations (solid), tropical continental locations (dashed-dotted), subtropical locations (dotted), and midlatitude locations (lowed dashed for original; upper dashed for adjusted).

6.0 flashes s^{-1}), improves the correlation factor from 0.37 to 0.52, but also leads to an increase of 1.2 flashes s^{-1} in the centered root mean square error. For the simulations in this paper, we opted for the increased variability, reduced biases, and improved correlations and set $\gamma = 2$, thus assuming that the flash frequency is proportional to $zmmu^2$.

[18] The local adjustment factor $\alpha_{i,j}$ is a grid box-specific (or region-specific) adjustment factor chosen so that the monthly average monthly flash rate for each grid box (or region) when averaged over a multiyear period (in this case 2001, 2004, 2005, and 2006) equals the v2.2 OTD/LIS climatological monthly average flash rate. The multiyear averaging allows for interannual variability in monthly average model flash frequencies.

[19] The adjustment factors are calculated in two steps. We begin by calculating a global adjustment factor (G) for each month. This factor is the amount that the multiyear average global sum of $(zmmu_{i,j} - threshold)_\gamma$ must be multiplied by in order to match the observed (v2.2 OTD/LIS climatology) global flash rate. This global factor is applied to each grid box (or region). We then calculate the local adjustment factors ($\alpha_{i,j}$) needed to best match the v2.2 OTD/LIS climatological monthly average flash rates at each grid point (or region). The value of $\alpha_{i,j}$ is an indicator of how well the parameterization is working (i.e., how closely flash rate and $[zmmu_{i,j} - threshold]_\gamma$ are related) and how well the model's convective parameterization captures the intensity and location of deep convection. In order to avoid very large values of $\alpha_{i,j}$, we constrained $\alpha_{i,j}$ to be between 0.02 and 20. In order to avoid very large flash rates, we also constrained the total flash frequency to be ≤150 flashes min^{-1} per 2° × 2.5° grid box. We then recalculated the global flash frequency and adjusted G to ensure that the model-calculated global flash frequency equaled the v2.2 OTD/LIS frequency of 46.3 flashes s^{-1}. This final adjustment to G does cause local flash frequencies to exceed 150 flashes min^{-1} at a few grid boxes (or regions).

[20] The initial parameterization used with the GEOS-4 meteorological fields included region-specific local adjustment factors and $\gamma = 1$. The eight regions were continental Africa (60°S–15°N, 30°W–45°E), continental South America (60°S–0°S, 130°W–30°W), continental North America (27.5°N–60°N, 130°W–60°W), continental southeast Asia (60°S–22.5°N, 45°E–180°E), continental north Asia/Europe (22.5°N–60°N, 30°W–160°E), coastal grid boxes, marine grid boxes, and the rest of the world. Continental grid boxes are 2° × 2.5° grid boxes that are within one grid box of a grid box that is at least 50% land. Coastal grid boxes are oceanic grid boxes that border continental grid boxes. Since biases at marine grid boxes were largest in the tropics and decreased with increasing latitudes, the marine adjustment factors also varied with latitude. They were largest in the tropics (10°S–10°N) and smallest in the midlatitudes (90°S–30°S, 30°N–90°N) with a linear decrease between the tropics and midlatitudes. The initial parameterization was used for the standard Aura4 GMI runs. It has since been replaced by the $\gamma = 2$ grid box-specific flash rate parameterization. This more recent parameterization was used in this paper and is expected to be used in all simulations driven by the GEOS-5 DAS.

[21] Modeling studies of *Ott et al.* [2010] are used as the basis to partition lightning NO in the vertical in the GMI model. Separate vertical profiles are used for tropical marine (15°S–15°N), tropical continental (15°S–15°N), subtropical (30°S–15°S, 15°N–30°N), and midlatitude (90°S–30°S, 30°N–90°N) grid boxes. The profiles specify the percentage of total NO mass deposited into 17 equally thick layers. The cloud top for each grid box with lightning is defined as the height at the top edge of the highest layer with detrainment. Figure 2 shows lightning NO emissions as a function

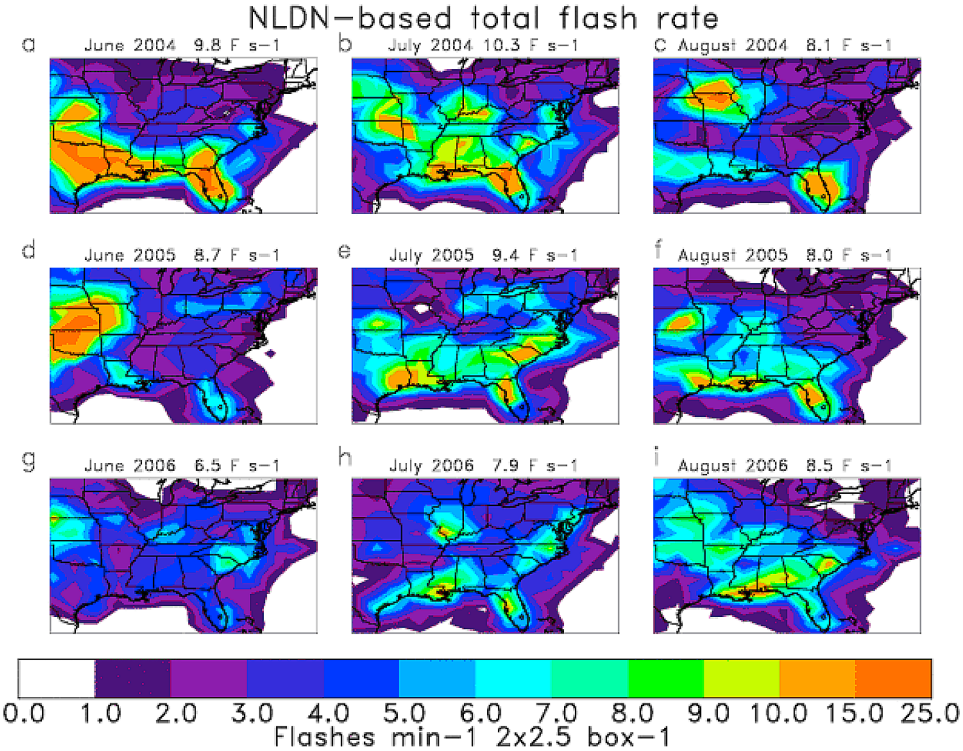

Figure 3. Monthly average NLDN-based total (CG + IC) flash rates for (top) June–August 2004, (center) June–August 2005, and (bottom) June–August 2006. Domain average flash rates for each month (flashes s^{-1}) are shown in the top right of each panel.

of altitude for each of the four different lightning NO regimes. The midlatitude and subtropical emission profiles are Gaussian in character with emissions peaking between 7 and 8 km. The tropical emission profiles are more skewed in character with continental emissions peaking at 12 km and marine emissions peaking at 10.5 km. Within the GMI model, these profiles are scaled to the GEOS-4 DAS cloud top heights on an individual grid cell basis.

[22] Recently, it has come to our attention that midlatitude convection often has subtropical characteristics during the summertime. Future GMI simulations driven with GEOS-4 or GEOS-5 meteorological fields will transition between the subtropical and midlatitude profiles at 40° during the summer season (June–September in Northern Hemisphere and December–March in Southern Hemisphere). In addition, the altitude of NO emissions for midlatitude storms will be shifted upward in the vertical by 1 km to better account for the surface elevation at the location of the *Ott et al.* [2010] midlatitude storms (see Figure 2). These profiles will be referred to as adjusted *Ott et al*. profiles in following sections.

[23] The total mass of nitrogen produced per second (LNO_x) is given by

$$LNO_x = [(f_{CG} \times LF \times E_{CG} + (1 - f_{CG}) \times LF \times E_{IC})] \times P \times CONV, \quad (2)$$

where LF is the total flash frequency (flashes s^{-1}), f_{CG} is the cloud-to-ground (CG) fraction, E_{CG} is the mean energy of a CG flash in joules (J), E_{IC} is the energy of an intracloud (IC) flash (J), P is the mean NO production rate per unit energy (molecules NO/J), and CONV is a conversion factor equal to the molecular weight of N (14 g/mol) divided by Avogadro's number (6.02×10^{-23} molecules/mol).

[24] The E_{IC}/E_{CG} ratio has been the subject of much recent research. Recent field studies including STERAO [*DeCaria et al.*, 2000, 2005], CRYSTAL-FACE [*Ott et al.*, 2010], and EULINOX [*Ott et al.*, 2007; *Fehr et al.*, 2004] have found that IC flashes are approximately as energetic as CG flashes [see also *Ridley et al.*, 2005]. Recent laboratory work by *Cooray et al.* [2009] also suggests that on average NO production by an IC flash is approximately equivalent to that of a CG flash. Assuming $E_{CG} = E_{IC}$ makes the estimation of f_{CG} unnecessary and reduces equation (2) to

$$LNO_x = LF \times PROD \times CONV, \quad (3)$$

where PROD (molecules NO/flash), the mean energy per flash, is the product of E and P. If we assume the global sum of LF equals 46.4 flashes s^{-1}, the global flash rate for version 2.2 of the OTD/LIS Low Resolution Annual Climatology (LRAC), we can adjust the value of PROD to obtain any desired global emission rate.

[25] The GMI model driven by GEOS-4 DAS fields was run for the 2004–2006 time period. For the "low NO_x" simulation discussed in this study, we set PROD equal to 1.47e26 molecules of NO per flash (240 mol per flash) resulting in a mean lightning NO emission rate of 5.00 Tg N/yr over the 4 year period. Global lightning NO emissions from this simulation were 4.30, 4.59, and 5.47 Tg N/yr for 2004, 2005, and 2006, respectively. The mean source during

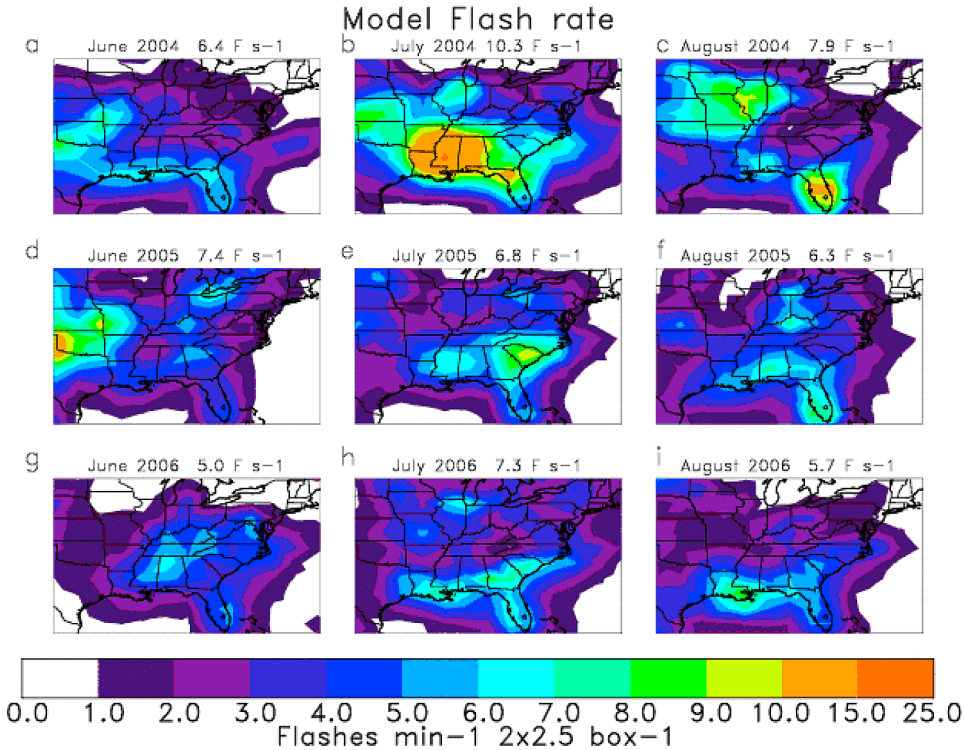

Figure 4. Monthly average model total (CG + IC) flash rates for (top) June–August 2004, (center) June–August 2005, and (bottom) June–August 2006. Domain-average flash rates for each month (flashes s^{-1}) are shown in the top right of each panel.

2004–2006 did not equal 5 Tg N/yr because the initial fit used meteorological fields from 2001, 2004, 2005, and 2006. For the "high NO_x" simulation we doubled PROD poleward of 24°. This 480 mol per flash extratropical source increased the global lightning NO source by approximately 30% and resulted in a global source of 5.71, 6.05, and 7.11 Tg N/yr for 2004, 2005, and 2006, respectively.

2.4. Evaluation of Spatial Flash Rate Distributions

[26] In order to evaluate the performance of the flash rate parameterization over the United States, model flash rates were compared to an independent data set. Figures 3a–3i show NLDN-based total flash rates over the United States during the summers of 2004, 2005, and 2006. Figures 4a–4i show model flash rates for the same time period. Overall, the spatial distributions and monthly variations of NLDN-based total flashes are reasonably well captured by the mass flux square based parameterization. The mean monthly spatial correlation equals 0.71 with correlations for individual months ranging from 0.58 during June 2006 to 0.80 during June 2004. Both NLDN-based and model flash rates are largest in a band that extends from southern Louisiana to central Florida although model flash rates are often 20%–40% too low in this region (e.g., June 2004 and to a lesser degree July and August 2005). Over the eastern United States (100°W–70°W, 25°N–50°N) model flash rates are 15%–25% smaller than NLDN-based flash rates with the low bias being largest during June 2004 (36%) and August 2006 (34%). The low bias with respect to the NLDN-based flash rates is likely due to the fact that NLDN-based flash rates show a yet unexplained high bias with respect to OTD/LIS long range monthly time series data [M. Martini, et al., The impact of North American anthropogenic emissions and lightning on long range transport of trace gases and their export from the continent during the summers of 2002 and 2004, submitted to *J. Geophys. Res.*, 2010]. *Jourdain et al.* [2010] also obtained higher monthly flash rates during July 2006 when they assumed an IC/CG ratio of 3 and scaled to NLDN observations instead of OTD/LIS observations. Therefore, investigators that use NLDN-based flash rates when studying the impact of lightning NO emissions on upper tropospheric photochemistry [e.g., *Cooper et al.*, 2006, 2009] are likely to predict a larger contribution from lightning NO than studies such as this one that scale to OTD/LIS flash rates.

[27] Both model and NLDN-based flash rates are largest over the region shown in Figures 3 and 4 during July 2004 and smallest during June 2006. Farther west, model and NLDN-based flash rates show a local maximum over the Sierra Madre mountain range in Mexico, especially during August 2005 and June–August 2006. This region of enhanced flash rates is associated with the North American monsoon. NLDN-based flash rates in this region are low because the NLDN does not have any sensors in Mexico, and detection efficiency falls off rapidly with distance from the United States.

3. Evaluation of GMI Simulations With Measurements

[28] In order to investigate the enhancement of tropospheric composition associated with lightning NO emis-

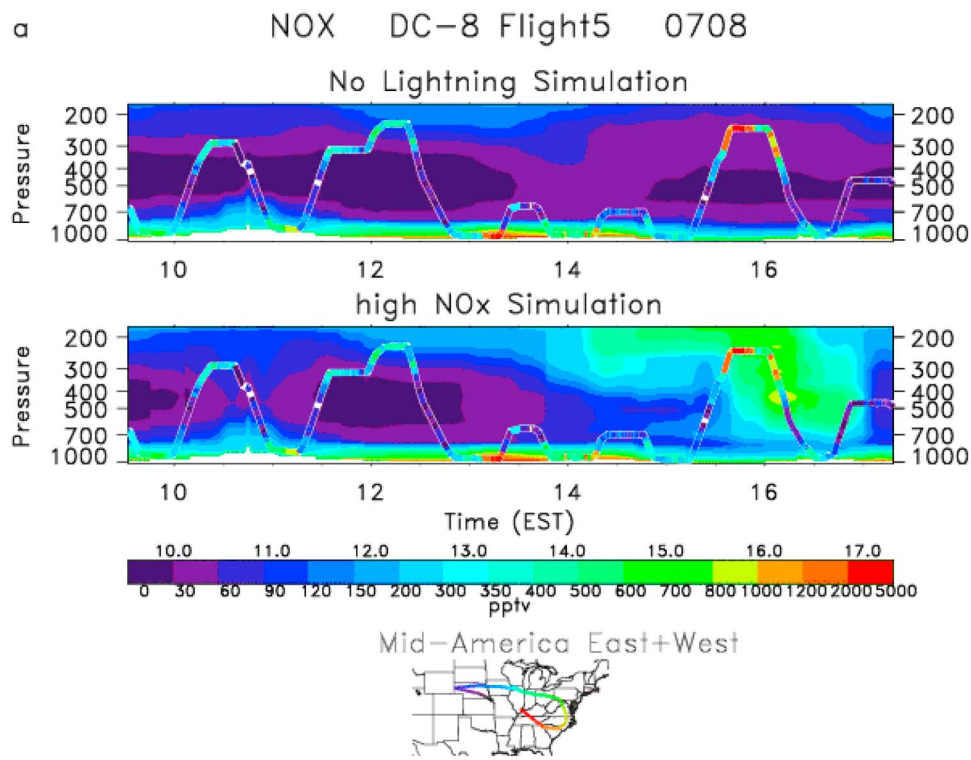

Figure 5. Curtain plot comparing (a) model NO_x and (b) ozone as a function of time (EST) and pressure (hPa) with measurements from DC-8 Flight 5 on 8 July 2004. Top shows results from simulation No Lightning. Bottom shows results from simulation high NO_x. Measured values are shown with a ribbon. Modeled values are shown in the background. The location and time of INTEX-A samples are shown on the U. S. map. The color bars shows the time of 1 min average samples and the scales (pptv for NO_x and ppbv for ozone).

sions, simulations of the 2004–2006 time period were run with varying amounts of lightning NO emissions. The first simulation ("No Lightning") did not include lightning NO emissions. The second simulation ("low NO_x") assumed 240 mol of NO were produced per flash. The third simulation ("high NO_x") included a doubled lightning NO emission source poleward of 24°. Although not strictly true due to the nonlinear nature of the ozone response to NO_x emissions, the lightning contribution to tropospheric composition is assumed to equal the difference between simulations with lightning NO emissions and the simulation without lightning NO emissions.

[29] The INTEX-A field campaign was conducted from 1 July to 15 August 2004 over North America and the western Atlantic [*Singh et al.*, 2006]. Its goals included source attribution. *Singh et al.* [2007] analyzed reactive nitrogen measurements during INTEX-A. They found unexpectedly large amounts of NO_x in the upper troposphere and suggested that lightning NO emissions are a "far greater contributor to NO_x in the upper troposphere than previously believed." Most modelers have found that increasing the lightning NO source substantially is necessary to bring model-calculated and measured NO_x during the INTEX-A campaign into agreement [*Hudman et al.*, 2007; *Pierce et al.*, 2007; *Bousserez et al.*, 2007; *Fang et al.*, 2010]. This increased lightning NO source is consistent with recent storm-scale field campaigns that indicate that lightning NO emissions from storms with midlatitude characteristics are larger than lightning NO emissions from storms with tropical characteristics [*Huntrieser et al.*, 2008; *Ott et al.*, 2010]. The *Ott et al.* [2010] cloud-resolved modeling and analysis of observed midlatitude and subtropical convective events has yielded a mean production per flash of 500 mol, which is similar to the value determined by *Hudman et al.* [2007]. The results of *Jourdain et al.* [2010] from a summer 2006 GEOS-Chem simulation in comparison with TES observations also corroborate the mean production of ~500 mol per flash.

3.1. Comparison With INTEX-A Measurements

[30] Before comparing with INTEX-A measurements, it is useful to compare the model lightning NO source with the lightning NO source used in other studies of this period. Lightning NO emissions over the contiguous United States during the INTEX-A time period equaled 0.17 Tg N for simulation low NO_x and 0.34 Tg N for simulation high NO_x. These values can be compared to the 0.27 Tg N contiguous U. S. INTEX-A lightning NO source used by *Hudman et al.* [2007, 2009] for their "improved (source) magnitude" simulation with GEOS-Chem and the 0.16 Tg N source used in RAQMS by *Pierce et al.* [2007].

[31] The primary aircraft used during INTEX-A was NASA's DC-8, and 1 min merge data sets are available for all species measured aboard the DC-8. We compared GMI

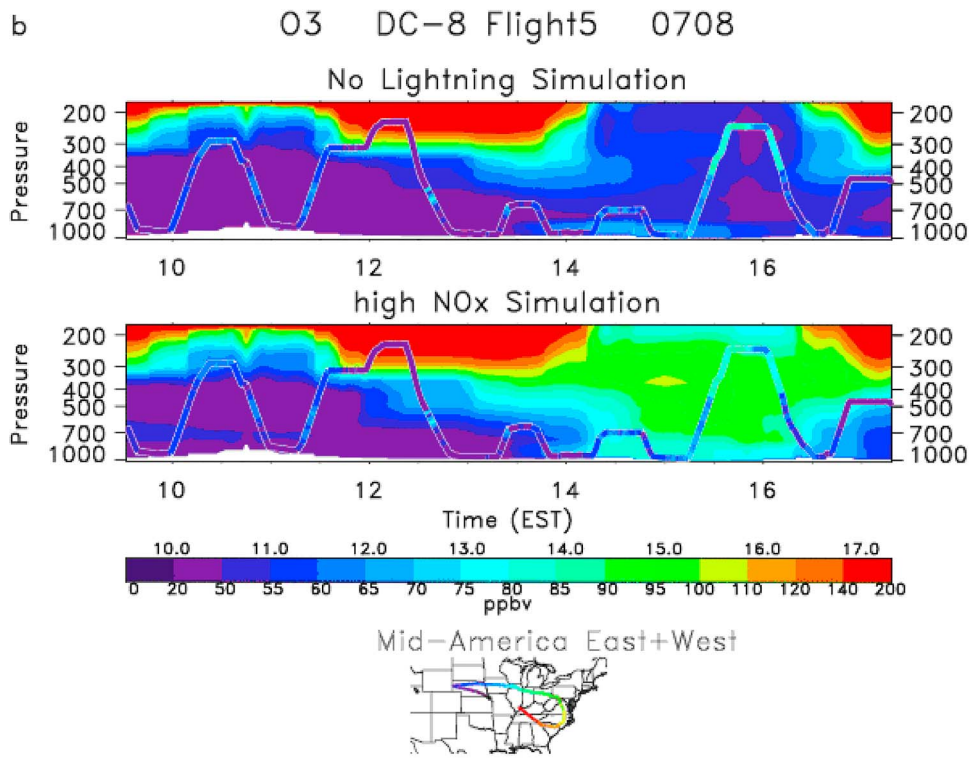

Figure 5. (continued)

output with these measurements after removing 1 min periods when contributions from fresh pollution, biomass burning, or stratosphere-troposphere exchange were greatly enhanced. Samples with greatly enhanced fresh pollution or biomass burning were removed as they are likely unrepresentative of a larger 2° × 2.5° grid box. Samples with a greatly enhanced stratospheric contribution were removed because this study focuses on the upper troposphere. The contribution of fresh pollution was deemed to be greatly enhanced when carbon monoxide (CO) mixing ratios exceeded 240 ppbv, ethane (C_2H_6) mixing ratios exceeded 3000 pptv or the acetylene (C_2H_2) to CO ratio exceeded 2. *Singh et al.* [2007] used the 240 ppbv CO and 3000 pptv C_2H_6 criteria for identifying INTEX-A periods with enhanced pollution. The C_2H_2 to CO ratio is often used as surrogate for air mass age because C_2H_2 and CO have different lifetimes (2 weeks for C_2H_2 and 2 months for CO) but similar combustion sources and OH sinks [e.g., *Xiao et al.*, 2007]. We did not use the NO_x/NO_y ratio as a fresh pollution indicator as its value during the INTEX-A period increased with increasing age in the upper troposphere and decreased with age in the lower and middle troposphere [see *Singh et al.*, 2007, Figure 4]. Following *Hudman et al.* [2007], we filtered out periods with biomass burning plumes as diagnosed by HCN > 500 pptv or CH_3CN > 225 pptv and stratospheric air as diagnosed by ozone/CO > 1.25 mol mol^{-1}. We also filtered out aircraft samples taken in the model stratosphere as diagnosed by comparing the aircraft sampling pressure with the GEOS-4 tropopause pressure available with the GMI output. When averaged over all of the INTEX-A DC-8 observations, the pollution, stratospheric, and biomass burning flags removed 1.6%, 2.8%, and 1.3% of the 1 min average samples, respectively. Overall, these three flags removed 5.7% of the samples. The tropopause pressure filter removed only 0.14% of samples. All subsequent comparisons are made using the filtered data sets.

[32] Nitric acid (HNO_3) measurements were made by the California Institute of Technology (CIT) using the chemical ionization mass spectrometry (CIMS) technique and by the University of New Hampshire (UNH) using a mist chamber/ion chromatograph (MC/IC) technique [*Singh et al.*, 2007]. Averaging over periods when both UNH and CIT measurements are available, UNH measurements are 10%–15% high with respect to CIT measurements in the lower and middle troposphere and approximately 40% low with respect to CIT measurements in the upper troposphere with a crossover point of approximately 5.5 km. UNH HNO_3 measurements will be used in this study as they are available for 96% of 1 min periods while CIT measurements are only available for 60% of the periods. The relatively large biases between these data products in the upper troposphere suggest that caution should be used when comparing model and measured HNO_3, NO_y, and NO_x/NO_y ratios in the upper troposphere. For example, UNH-based NO_x/NO_y ratios in the upper troposphere are approximately 10% larger than CIT-based NO_x/NO_y ratios.

[33] Figures 5a and 5b compare model NO_x and ozone from simulations No Lightning and high NO_x to 1 min average DC-8 measurements during INTEX-A flight 5 on 8 July 2004. Only periods when NO, NO_2, and ozone measurements are all available were considered. Lightning

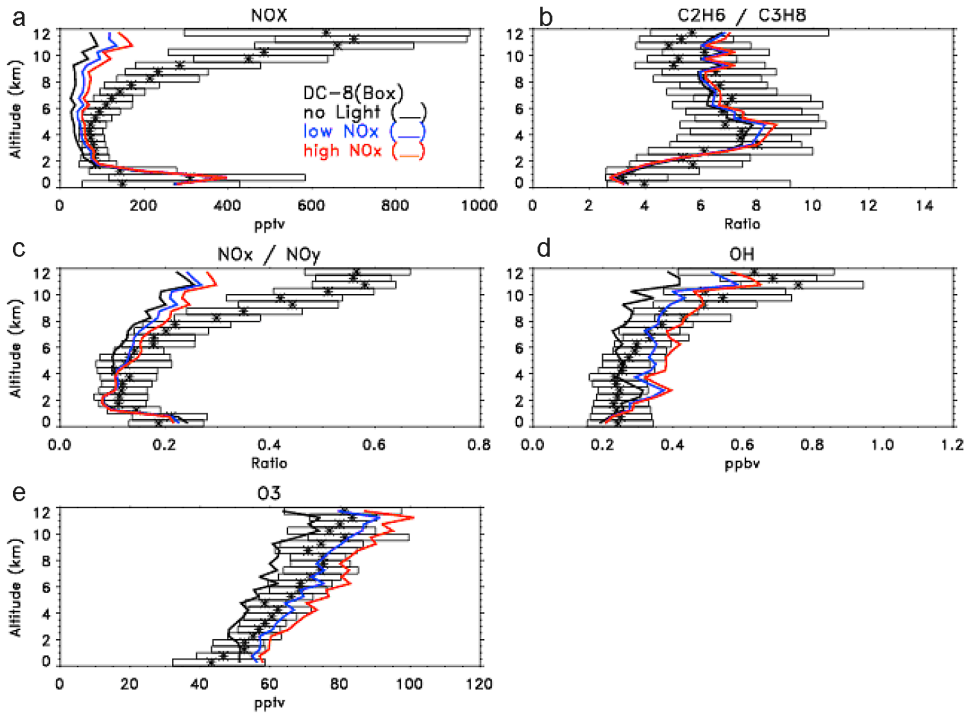

Figure 6. Mean model versus observed profiles of (a) NO_x, (b) C_2H_6/C_3H_8, (c) NO_x/NO_y, (d) OH, and (e) ozone during the INTEX-A field campaign. Means are calculated using data from 18 flights between 1 July and 14 August. Observed median mixing ratios within 0.5 km vertical bins are shown with an asterisk, while bars show the 25th and 75th percentiles. Model median mixing ratios for simulations No Lightning, low NO_x, and high NO_x are shown in black, blue, and red, respectively. Model profiles were obtained by sampling daily 13:30 LT GMI files at the location (9-pt 1/distance square weighting used) and altitude (linear interpolation in height used) of the aircraft.

NO emissions are responsible for the observed 16:00 EST peak in upper tropospheric NO_x. Measured NO_x mixing ratios were highest between 15:33 and 16:10 EST when they exceeded 350 pptv. During this period, the DC-8 flew 430 km in a southwesterly direction between Goldsboro, NC (78.0°W, 35.1°N) and Greenville, SC (82.6°W, 34.6°N) while ascending from 350 to 240 hPa before descending to 390 hPa. The median observed NO_x value during this period equaled 963 pptv, while model medians equaled 45, 280, and 703 pptv for simulations No Lightning, low NO_x, and high NO_x, respectively. Enhancement factors of model NO_x with respect to the no-lightning simulation at the location of one-minute samples during this period ranged from 2.9 to 8.9 (6.8–24.2) for the low NO_x (high NO_x) simulation. As expected, ozone was also enhanced during this period. The median ozone mixing ratio during this period along this flight path equaled 80 ppbv. Model medians equaled 50, 78, and 88 ppbv for simulations No Lightning, low NO_x, and high NO_x, respectively. Upper tropospheric NO_x amounts were enhanced to a lesser degree from 10 to 10:30 and 11:30 to 12:30 EST. These regions of enhanced NO_x were not captured by the model as it did not place convection at the right location and time leading to a substantial underestimation of NO_x by the model when averaged over the entire flight path.

[34] The underestimation of upper tropospheric NO_x is also seen on several other flights. Figure 6a compares mean model NO_x profiles with the mean profile from the INTEX-A field campaign. At altitudes above 9km, mean measured NO_x equals 557 pptv, while model NO_x ranges from 110 pptv for simulation low NO_x to 157 pptv for simulation high NO_x. Averaged over all DC-8 flight track samples, model NO_x for simulation low NO_x (high NO_x) is a factor of 2.7 (1.7) too low for 7–9 km and a factor of 5.1(3.6) too low for 9–12 km. Substantial underestimations were also seen at the 10th, 25th, 50th, 75th, and 90th percentiles of the NO_x distribution. Simulations with GEOS-Chem [*Hudman et al.*, 2007], RAQMS [*Pierce et al.*, 2007], Modélisation de la Chimie Atmosphérique Grande Echelle (MOCAGE) [*Bousserez et al.*, 2007], and MOZART-4 [*Fang et al.*, 2010] were also unable to reproduce observed NO_x amounts in the upper troposphere during the INTEX-A field experiment. The GEOS-Chem simulations were driven with the same meteorological fields and used a very similar chemical mechanism as the GMI model. NO_x in the improved source GEOS-Chem simulation was approximately a factor of 1.7 too low for 7–9 km and a factor of 2.2 too low for 9–12 km. Biases in the GEOS-Chem simulation were largest in the Midwest and were partially attributed to an underestimation of flash rates within GEOS-Chem. The RAQMS simulations were initialized with GFS fields and used an updated version of the CBMZ chemical mechanism; Upper tropospheric NO_2 was approximately a factor of 2 too low. Low biases in MOCAGE ranged from approximately a factor of two at 9 km to a factor of 4 at 11 km.

[35] The underestimation of upper tropospheric NO_x may be partially caused by an underestimation of the vertical

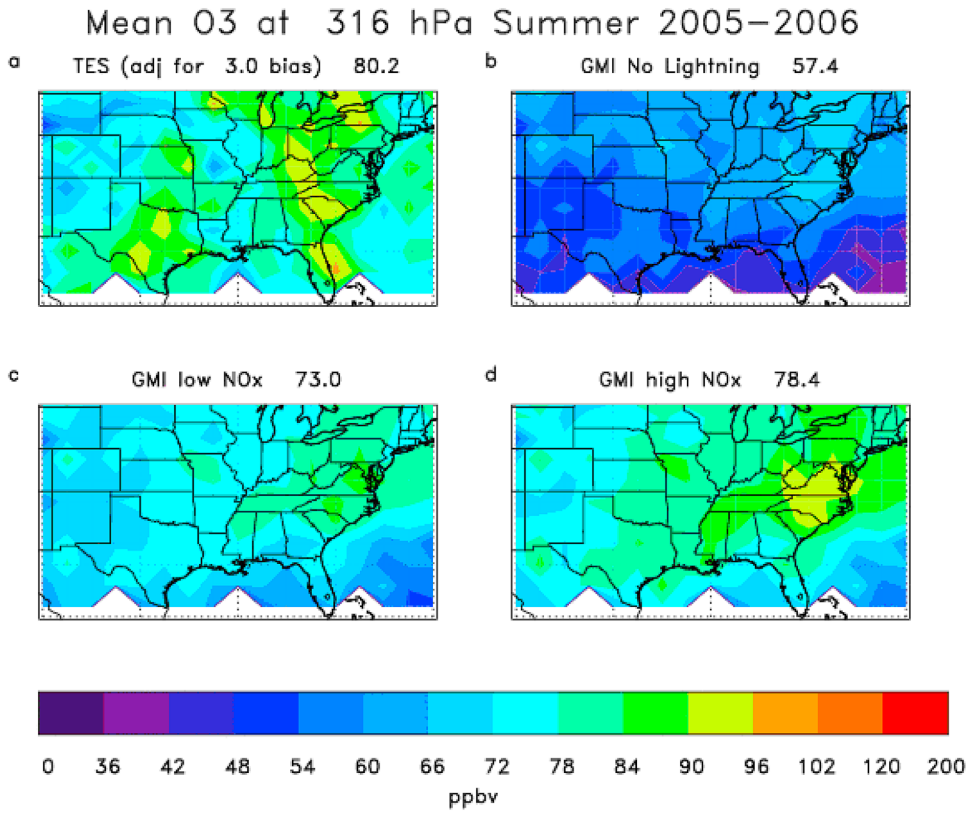

Figure 7. Mean summer 2005–2006 316 hPa ozone (ppbv): (a) TES-retrieved ozone after adjusting TES for 3 ppbv positive bias, (b) model ozone from simulation No Lightning, (c) model ozone from simulation low NO_x, and (d) model ozone from simulation high NO_x. Mean mixing ratio over domain is shown in upper right.

extent of deep convection in the GEOS-4 DAS. Figure 6b compares model and measured ratios of ethane (C_2H_6) to propane (C_3H_8) during INTEX-A. Both ethane and propane have surface sources; however, the lifetime of propane is 1–2 weeks while the lifetime of ethane is 5 × greater [*Wang and Zeng*, 2004]. Therefore, the ratio of ethane to propane increases as air masses age. During the INTEX-A mission, the measured ratio was 3–4 in the boundary layer, 7–8 in the midtroposphere, and 5–6 in the upper troposphere [see also *Zhao et al.*, 2009]. Upper tropospheric air has a lower mean age than midtropospheric age due to periodic rapid injection of boundary layer air by deep convection. The model ethane to propane ratio agrees very well with INTEX-A measurements except in the upper troposphere. In this 10.5–12 km region, the model shows a high bias of 10%–20%. While small, this high bias suggests that the injection of boundary layer air and lightning NO emissions into these layers by deep convection is underestimated. *Hudman et al.* [2007] lessened the impact of this possible bias in convective cloud top heights by assuming lightning-producing storms extend to the tropopause. This assumption led to better agreement with INTEX-A measurements. *Bousserez et al.* [2007] also noted that the agreement between NO from MOCAGE and NO from INTEX-A would have been better if model-calculated convective clouds extended to a higher altitude.

[36] In order to investigate the sensitivity of the upper tropospheric low bias to the vertical partitioning of lightning NO emissions, high NO_x simulations were run for 2004 using the *Pickering et al.* [1998] and the adjusted *Ott et al.* [2010] (see section 2.3) profiles. Averaged over all DC-8 flight track samples, model NO_x for the NO_x simulation with the adjusted *Ott et al*. (*Pickering et al.*) profiles is a factor of 1.4 (1.2) too low for 7–9 km and a factor of 2.8(2.2) too low for 9–12 km. These biases can be compared with the 1.7 and 3.6 for the original *Ott et al*. profiles. Biases with respect to the INTEX-A NO_x measurements are smaller because these profiles place 26% (43%) of their emissions above 9.5 km, for a 17 km cloud, while the *Ott et al*. profile places 17% of its emissions above this level. After including the uncertainty resulting from vertical partitioning of emissions, we conclude that upper tropospheric NO_x is a factor of 1.2–1.7 too low for 7–9 km and a factor of 2.2–3.6 too low for 9–12 km. These differences in partitioning are also likely to explain the upper tropospheric NO_x low bias GMI shows with respect to GEOS-Chem.

[37] Figure 6c compares model NO_x/NO_y ratios from simulations No Lightning, low NO_x, and high NO_x to observed ratios calculated using UNH HNO_3. Model means were obtained by sampling monthly average (July or August as appropriate) NO_x and NO_y fields at the location of INTEX-A measurements. Monthly average fields were sampled because HNO_3 and PAN were not contained in the daily GMI overpass fields (see Appendix A). With the exception of the boundary layer, model NO_x/NO_y ratios are biased low with respect to UNH ratios. As expected, the high NO_x simulation with the GMI model does the best job of capturing the

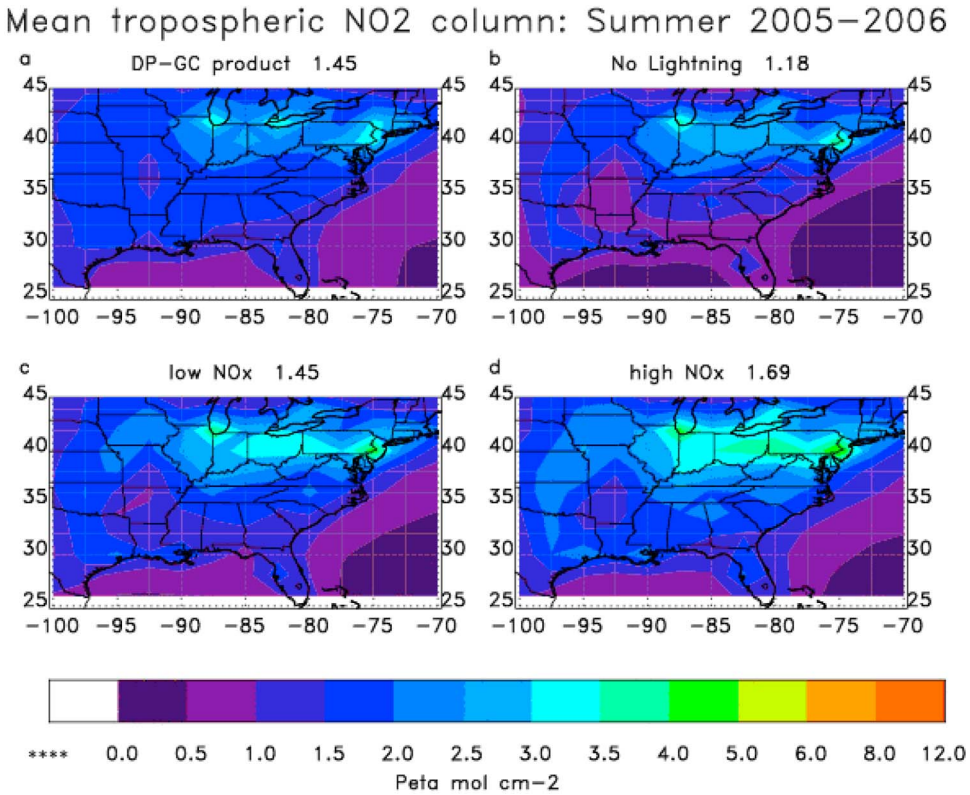

Figure 8. Mean tropospheric NO_2 columns for June–August 2005–2006 from the (a) DP-GC product, (b) GMI simulation No Lightning, (c) GMI simulation low NO_x, and (d) GMI simulation high NO_x.

vertical profile of NO_x/NO_y. Low-biases for this simulation are 5%–10% in the lower and midtroposphere increasing to 40%–50% in the upper troposphere. Actual upper tropospheric biases are likely to exceed what is shown here because monthly averaging removes the diel cycle of the NO_x/NO_y ratio and most of the measurements were taken during the late morning and early afternoon when NO_x/NO_y ratios are lower than diel averages. For example, model upper tropospheric NO_x/NO_y ratios at ten eastern U. S. sites during July 2004 have a 15%–30% low bias with respect to the diel mean between 18 and 24 UT and a 15%–30% high bias with respect to the diel mean between 06 and 12 UT. Low biases of 20% are typical at the mean INTEX-A sampling time of 18 UT. Adjusting the NO_x/NO_y ratios for the diel bias would increase upper tropospheric low biases to 50%–60%. Biases in upper tropospheric HNO_3 are relatively small with simulation low NO_x agreeing best with the UNH measurements and simulation high NO_x agreeing best with the CIT measurements (not shown). Model PAN is approximately 30% lower than measured PAN in the upper troposphere (not shown). Figure 6d compares model OH at the time of the INTEX-A measurements with measured OH. Biases in the boundary layer (0–2 km) are small although model OH increases with altitude while measured OH is nearly constant with altitude. The increase in model OH with altitude results in a 27% (41%) high bias for simulation low NO_x (high NO_x) in the middle troposphere (2–7 km). Observed OH increases more rapidly with height than model OH in the mid and upper troposphere. This difference in slope leads to a relatively small 16 (2%) high bias in the upper troposphere (7–12 km) for the low NO_x (high NO_x) simulation. The relatively small bias in model OH indicates that excessive upper tropospheric model OH is not the cause of the low bias in model NO_x.

[38] The underestimation of upper tropospheric NO_x and the NO_x/NO_y ratio is consistent with too rapid conversion of NO_x to HNO_3 and PAN in the model and may indicate a fundamental problem with upper tropospheric NO_y chemistry. *Henderson et al.* [2010] evaluated upper tropospheric NO_y chemistry using seven different chemical mechanisms and an observation-based aging model. They found that each of the models overestimated PAN and the rate of conversion from NO_x to HNO_3.

[39] Despite the underestimation of NO_x, model ozone agrees well with or is a bit higher than measured ozone in the upper troposphere (Figure 6e). Biases range from −3% to 10% for simulation low NO_x to 6%–23% for simulation high NO_x. The GMI simulation without lightning NO emissions has a 10%–22% low bias above the boundary layer. Surprisingly, both the measurements and the model show a decrease in ozone in the uppermost observational layer (11.5–12.0 km). The cause of the decrease is unclear, but it does appear to be robust. The average in this layer was calculated using 260 samples from 15 different flights.

[40] Doubling the extratropical lightning NO source as is done in simulation high NO_x introduces a high bias in mid to upper tropospheric ozone at the location of INTEX-A samples. This increase in bias argues against a doubled

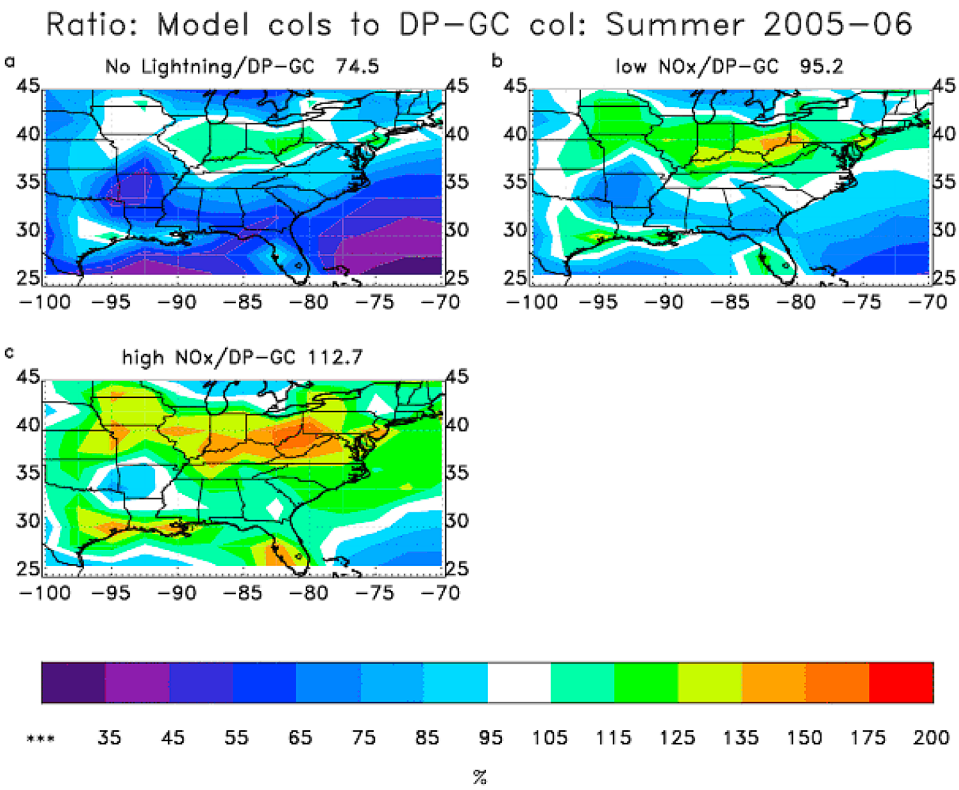

Figure 9. Mean ratios between various model columns and the DP-GC tropospheric NO_2 column for June–August 2005–2006: (a) No Lightning/DP-GC product, (b) low NO_x/DP-GC product, and (c) high NO_x/DP-GC product.

extratropical lightning NO source. However, excessive stratosphere-troposphere exchange, excessive vertical diffusion, insufficient convection, and/or insufficient vertical resolution could all contribute to high biases for ozone in the upper troposphere. *Considine et al.* [2008] compared mean monthly tropopause level ozone amounts from a multiyear GMI combo model simulation driven by GCM fields with ozonesonde measurements at nine Northern Hemisphere midlatitude locations including Wallops Island, Virginia. This simulation used a cloud top height based flash rate parameterization [*Price and Rind*, 1992] and climatological monthly average ISCCP cloud top heights. In general, model ozone amounts showed a high bias of 40%–60% at the tropopause. At Wallops Island, a substantial high bias was present during the fall through spring but not during the summer months comprising the INTEX-A period. During this period of limited STE, biases were relatively small and mostly associated with differences between the observed and modeled tropopause pressures. While the seasonal cycle of the biases at Wallops Island indicates a STE component, [*Considine et al.*, 2008] argue that the most likely cause of the midlatitude high biases is insufficient vertical resolution and/or excessive diffusion near the tropopause. Given the many processes that could impact upper troposphere ozone, we do not believe that the increasing high bias is a strong argument against the high NO_x source. In order to investigate this further, we will now compare model upper tropospheric ozone with satellite retrievals from the Tropospheric Emission Spectrometer (TES).

3.2. Comparison With Aura Measurements

[41] The Tropospheric Emission Spectrometer (TES) aboard NASA satellite Aura (launched 15 July 2004) retrieves ozone from the 9.6 μm ozone absorption band. *Nassar et al.* [2008] validated TES retrievals using ozonesonde measurements. Overall, they found that TES retrievals have a positive bias of 3–10 ppbv, although biases varied latitudinally and seasonally. Mean summertime biases in the northern midlatitudes ranged from 5 to 10 ppbv in the lower troposphere to about 3 ppbv in the upper troposphere.

[42] Figures 7a–7d compare TES-retrieved and model 316 hPa mean summertime ozone for the 2005–2006 time period. The mean TES plots were created by mapping TES global survey observations onto the 2° × 2.5° GMI grid after removing suspect observations. Observations were flagged as suspect if any of the following were true: (1) retrieval quality master flag of zero, (2) C curve criteria satisfied, or (3) surface mixing ratio exceeding 200 ppbv. C curve retrievals are retrievals with anomalously high ozone near the surface and anomalously low ozone in the middle troposphere. The C curve test of *L*. Zhang was used in this study [see *Osterman et al.*, 2009]. In order to account for biases in the TES retrievals, ozone values in the 316 hPa TES plot were reduced by 3 ppbv before plotting. Model output was passed through the TES averaging kernel before comparisons.

[43] In general, both TES-retrieved and model 316 hPa ozone increases from west to east over the eastern United States. The mean difference between model and TES-

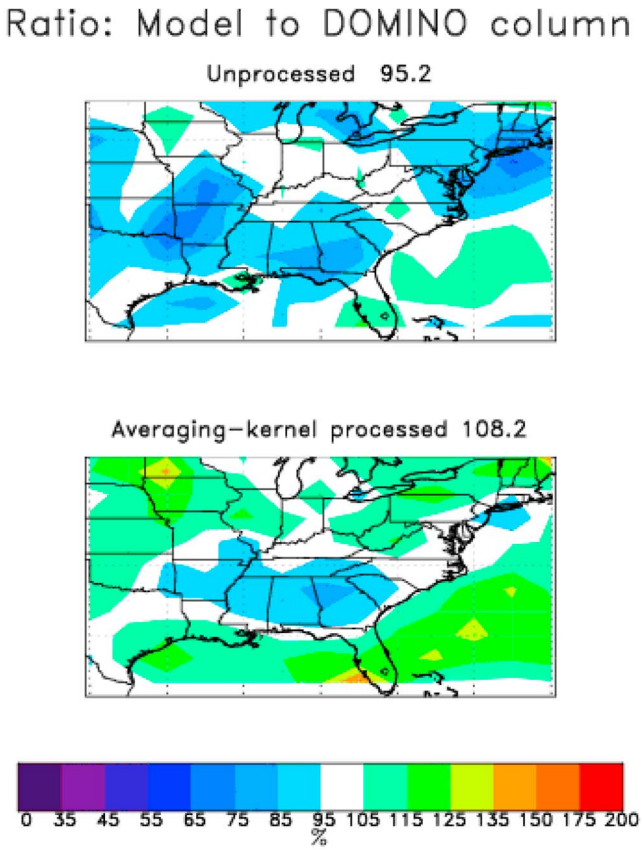

Figure 10. Ratio between model tropospheric NO_2 columns and mean satellite-retrieved DOMINO column for summer months during 2005–2006: (a) unprocessed high NO_x column and (b) processed high NO_x column.

retrieved ozone (after the 3 ppbv adjustment) is a 7 ppbv (2 ppbv) low bias for the low-NO_x (high-NO_x) simulation. Therefore, the high-NO_x simulation yields the best agreement with TES upper tropospheric ozone. *Jourdain et al.* [2010] found that the low bias of GEOS-Chem with respect to TES upper tropospheric ozone over the United States during July 2006 decreased from 12–22 ppbv to 6–18 ppbv with a doubled lightning NO source. They cautioned that several other factors may also contribute to the low bias including an underestimation of STE, PBL ventilation, or precursor emissions. The mean enhancement of 316 hPa ozone associated with lightning NO emissions equals 16 (21) ppbv for the low-NO_x (high-NO_x) GMI simulation.

[44] The Ozone Monitoring Instrument (OMI) aboard the Aura satellite measures direct and backscattered sunlight in the ultraviolet-visible range. It retrieves NO_2 with a resolution of up to 13 km × 24 km. Four tropospheric NO_2 products are currently available. These products are the OMI standard product [*Bucsela et al.*, 2008; *Celarier et al.*, 2008], the DOMINO product [*Boersma et al.*, 2007], the DOMINO/GEOS-Chem product (DP-GC) [*Lamsal et al.*, 2010], and the University of Bremen product [*Kim et al.*, 2009]. Each of these algorithms begins with the same slant column but differ in their separation of the stratospheric column from the tropospheric column and in their calculation of the tropospheric air mass factor. These differences lead to substantially different tropospheric column amounts [e.g., *Bucsela et al.*, 2008]. Lamsal et al. (submitted manuscript, 2009) compare the standard, DOMINO, and DP-GC products to each other and to indirect estimates of columns based on bottom-up emission inventories and in situ surface layer measurements. Over North America, they found that the mean tropospheric summertime NO_2 column from the standard product has a 22% high bias with respect to the DOMINO product and a 67%–74% high bias with respect to the inferred columns. The DOMINO column has a 25%–33% high bias with respect to the inferred columns, while the DP-GC product has only a 5% low bias with respect to the inferred columns. We will primarily use the DP-GC product in this study; however, we will also use version 1.0.2 of the DOMINO product as it is the only product that has readily available averaging kernels.

[45] Figures 8a–8d compare the satellite-retrieved DP-GC mean summer 2005–2006 tropospheric NO_2 column over the eastern United States (a) with columns from simulations No Lightning (b), low NO_x (c), and high NO_x (d). Model columns were obtained by integrating model output at the time of the afternoon Aura overpass from the surface to 150 hPa. Mean model columns were obtained by averaging model columns on days when the DP-GC product was available. When averaged over the entire domain, the mean column from simulation low NO_x (1.45 Peta mol cm^{-2}) agrees with the DP-GC column (also 1.45 Peta mol cm^{-2}); however, the agreement masks a high bias in the northern portion (36°N–45°N) of the domain centered over the Ohio River Valley and a low bias in the southern portion (25°N–35°N) of the domain. Figure 9 shows ratios between model columns and the DP-GC product. The mean bias in the northern portion of the domain equals −13%, 3%, and 18% for simulations No Lightning, low NO_x, and high NO_x, respectively. The mean bias for the southern portion of the domain equals −38%, −13%, and 7%, respectively. Doubling the midlatitude lightning NO source improves the agreement with DP-GC columns in the southern United States, although a minor low bias still exists over south central states centered over Arkansas possibly due to an underestimation of flash rates by GMI over this region compared with the adjusted NLDN data, but exacerbates high biases with respect to the DP-GC columns over the northeastern United States. The Ohio River Valley centered high bias over the northern portion of the domain is at least partially due to an overestimate of anthropogenic NO emissions in this region by GMI. Model NO emissions over the United States were decreased uniformly by 22% from NEI99 values to obtain year 2004 emissions (see section 2.1), although CEMS data indicates that reductions were largest over the Ohio River Valley, and emissions continued to decrease from 2004 to 2006. Overall, the spatial pattern of the biases is consistent with the high NO_x lightning source and an overestimated anthropogenic source.

[46] Figures 10a and 10b show the ratio between the model tropospheric column from simulation high NO_x and the DOMINO column over the eastern United States during the summers of 2005 and 2006. Ratios are shown before (Figure 10a) and after (Figure 10b) application of the averaging kernel to the GMI fields (see Appendix A). Overall, application of the kernel increased the model column and changed the mean 5% low bias with respect to the

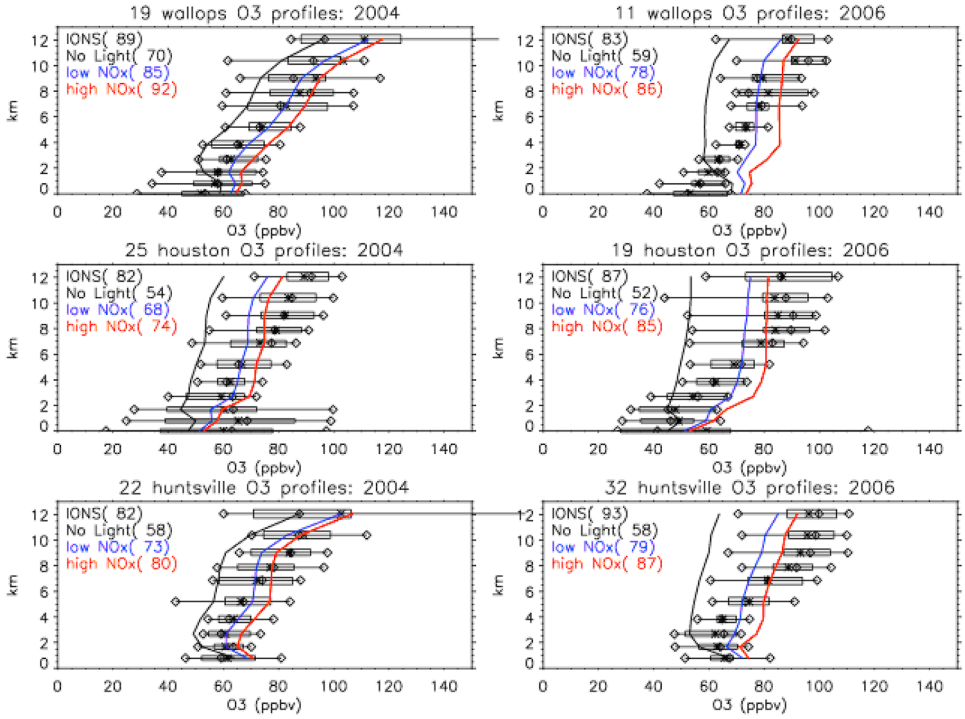

Figure 11. Mean summertime profiles of ozone at (top) Wallops Island, VA (75.7°W, 37.9°N); (middle) Houston, TX (95.3°W, 29.72°N); and (bottom) Huntsville, AL (86.64°W, 34.72°N) for (left) 2004 and (right) 2006. Measured profiles taken as part of the IONS campaign. GMI-calculated profiles from simulations No Lightning, low NO_x, and high NO_x. Smoothed IONS profiles for each day were obtained by averaging measurements within pressure bins defined by the vertical resolution of the GMI time series data sets. The 11 layers shown correspond to pressure layers centered at 1000, 900, 800, 700, 600, 500, 400, 350, 300, 250, and 200 hPa. Bars (whiskers) show the 25th and 75th (10th and 90th) percentiles of the smoothed daily profiles. An asterisk shows the median observed ozone mixing ratio for each pressure layer. Mean mixing ratios of the highest seven layers (approximately 7–12 km) are shown in parentheses.

DOMINO column to a mean 8% high bias with respect to the DOMINO column. In general, application of the averaging kernel can increase or decrease model columns depending on the vertical distribution of model trace gases. Application of the averaging kernel to simulation No Lightning decreased the mean column and increased the low bias with respect to DOMINO from 37% to 43%. Of course, this finding is not surprising. A priori assumptions about the vertical distribution of a retrieved constituent are necessary in order to accurately retrieve column amounts.

[47] Processing of the GMI field using the DOMINO averaging kernel increased the NO_x column in simulation high NO_x. This enhancement would increase the small (7%) model high bias with respect to the DP-GC product in the southern United States. Thus, it appears that the best agreement between the DP-GC product and the GMI model would be obtained with a midlatitude lightning NO source that is slightly less than the 480 mol per flash of the high-NO_x simulation. *Zhao et al.* [2009] also found an inconsistency between the lightning NO source that minimizes biases with respect to upper tropospheric measurements and the source that minimizes differences with respect to tropospheric columns. They used INTEX-A measurements and columns from the Scanning Imaging Absorption Spectrometer for Atmospheric Cartography (SCIAMACHY) [*Martin et al.*, 2006].

3.3. Comparison With IONS Ozone Profiles

[48] During the summers of 2004 and 2006 as part of the INTEX Ozonesonde Network (IONS) several hundred ozonesondes were launched from North American sites across the southern and eastern United States [*Thompson et al.*, 2007a, 2007b]. Figure 11 compares mean IONS summertime profiles at Wallops Island, VA (75.7°W, 37.9°N); Houston, TX (95.3°W, 29.72°N); and Huntsville, AL (86.64°W, 34.72°N) with mean profiles from GMI simulations No Lightning, low NO_x, and high NO_x at the same locations. Lightning NO emissions are an important contributor to the ozone profiles at each of these sites with the mean upper tropospheric (7–12 km) summertime enhancement of ozone associated with lightning NO for simulation high NO_x equaling 21 ppbv in 2004 and 30 ppbv in 2006.

[49] Upper tropospheric biases between the GMI simulations and IONS are summarized in Table 1. Mean upper tropospheric profiles from simulation No Lightning have a low bias of 19–35 ppbv with respect to the IONS profiles. Overall, simulation high NO_x provides the best agreement with measurements. At Wallops Island, model upper tro-

Table 2. Measured and Modeled Difference (ppbv) Between Summer 2006 and Summer 2004 Upper Tropospheric Ozone at IONS Sites[a]

	IONS	No Lightning	Low NO_x	High NO_x
Wallops	−6	−11	−7	−6
Houston	+5	−2	+8	+11
Huntsville	+11	+0	+6	+7

[a]From left, IONS measurements, simulation No Lightning, simulation low NO_x, and simulation high NO_x.

pospheric ozone amounts have a 4–5 ppbv low bias for simulation low NO_x and a 3 ppbv high bias for simulation high NO_x. At Houston, TX, a low bias of 11–14 (2–8) ppbv is seen for the low NO_x (high NO_x) simulation. At Huntsville, the low biases are 9–14 ppbv for the low NO_x simulation and 2–6 ppbv for the high NO_x simulation. The low biases at Houston and Huntsville are at least partially due to the underestimation of flash rates by GMI in the southern United States.

[50] Measurements show an increase in upper tropospheric ozone between 2004 and 2006 at Houston (5 ppbv) and Huntsville (11 ppbv) (see Table 2). The GMI simulation without lightning NO emissions does not show this increase. In this simulation, mixing ratios at Houston decrease by 2 ppbv and are unchanged at Huntsville. The GMI simulations with lightning NO emissions do capture this interannual signal. For the high-NO_x simulation, upper tropospheric model ozone amounts increase by 11 ppbv at Houston and 7 ppbv at Huntsville. Apparently, a 13 ppbv (7 ppbv) change in the ozone produced from lightning NO emissions is responsible for the increases in ozone at Houston (Huntsville) between 2004 and 2006. Observed ozone amounts at Wallops Island decrease by 6 ppbv between 2004 and 2006; however, the GMI simulations indicate that the decrease would have been even larger (perhaps 11 ppbv) if not for an 5 ppbv increase in the contribution of lightning NO between 2004 and 2006. For the high-NO_x simulation, lightning NO contributed 22 ppbv during 2004 and 27 ppbv during 2006. The increased contribution of lightning NO to the ozone budget during 2006 did not result from an increase in the lightning NO source between 2004 and 2006. NLDN-based (model) flash rates in July 2004 averaged 12.9 (12.2) flashes per second while NLDN-based (model) flash rates in July 2006 averaged 10.3 (10.0) flashes per second. *Cooper et al.* [2009] used a Lagrangian approach to evaluate 2004–2006 differences in ozone profiles at IONS sites. They also found more ozone in 2006 but less NO emissions. They attributed the cause to weather. Weather conditions in 2006 were more conducive to ozone formation than weather conditions in 2004. In a typical summer, an upper tropospheric anticyclone forms over northern Mexico and the southern United States. This anticyclone lessens outflow from the United States and leads to a build up of lightning NO produced ozone over the southern United States. In 2004, this anticyclone was weaker and further south than normal. In 2006, this anticyclone was stronger than average and positioned further north. Recirculation was enhanced in 2006 compared to 2004. This enhancement increased the residence time of

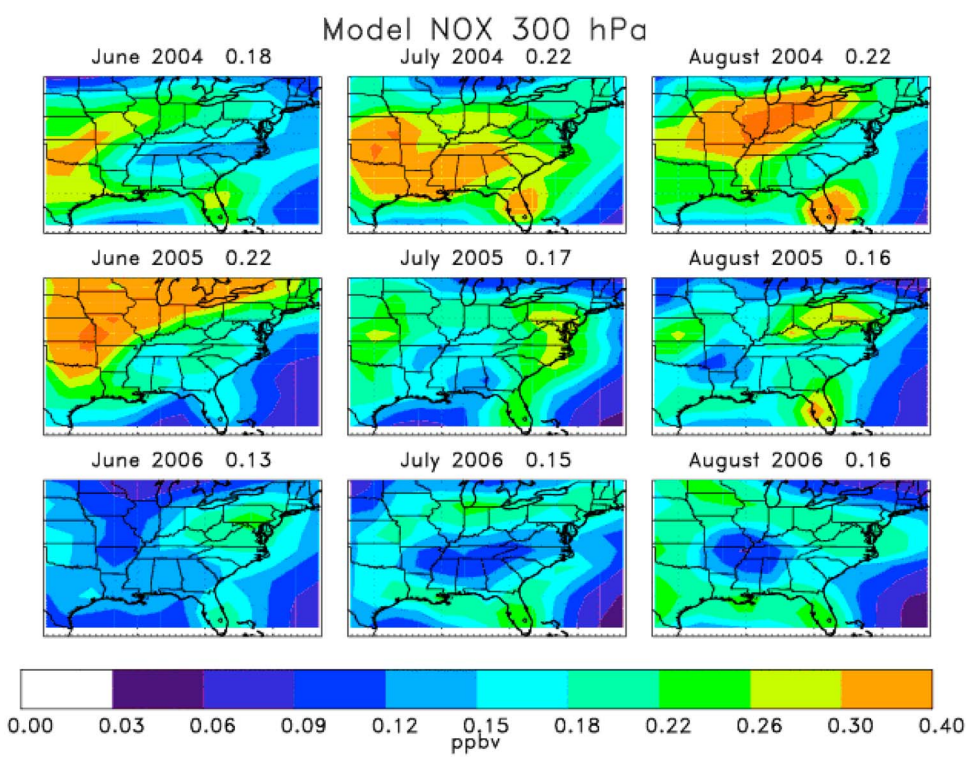

Figure 12. Upper tropospheric (300 hPa) mixing ratios of NO_x (ppbv) from GMI simulation high NO_x for (top) June, July, and August 2004; (middle) June, July, and August 2005; and (bottom) June, July, and August 2006.

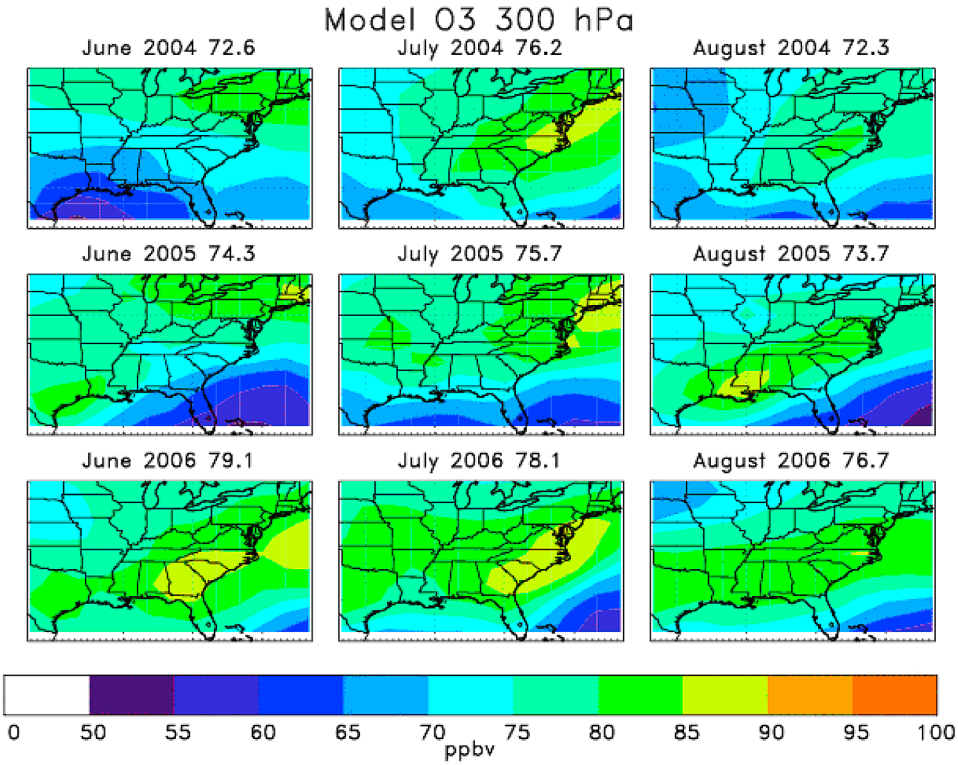

Figure 13. Upper tropospheric (300 hPa) mixing ratios of O_3 (ppbv) from GMI simulation high NO_x for (top) June, July, and August 2004; (middle) June, July, and August 2005; and (bottom) June, July, and August 2006.

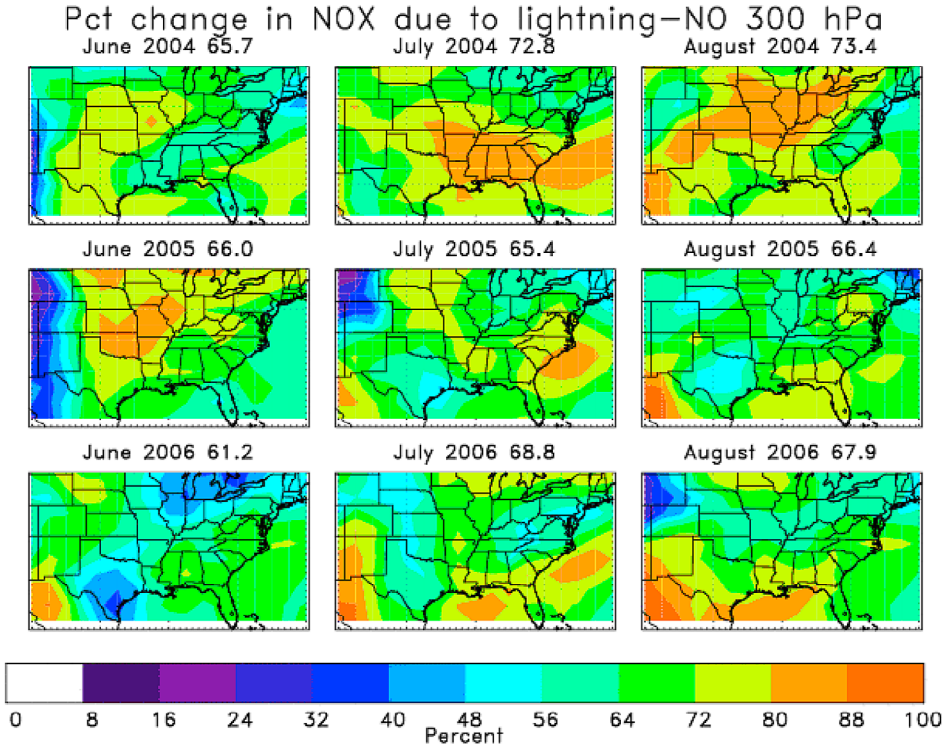

Figure 14. Percentage of 300 hPa NO_x due to lightning NO emissions during (top) June, July, and August 2004, (middle) June, July, and August 2005, and (bottom) June, July, and August 2006. Results shown obtained by dividing differences between simulations high NO_x and No Lightning by results from high NO_x.

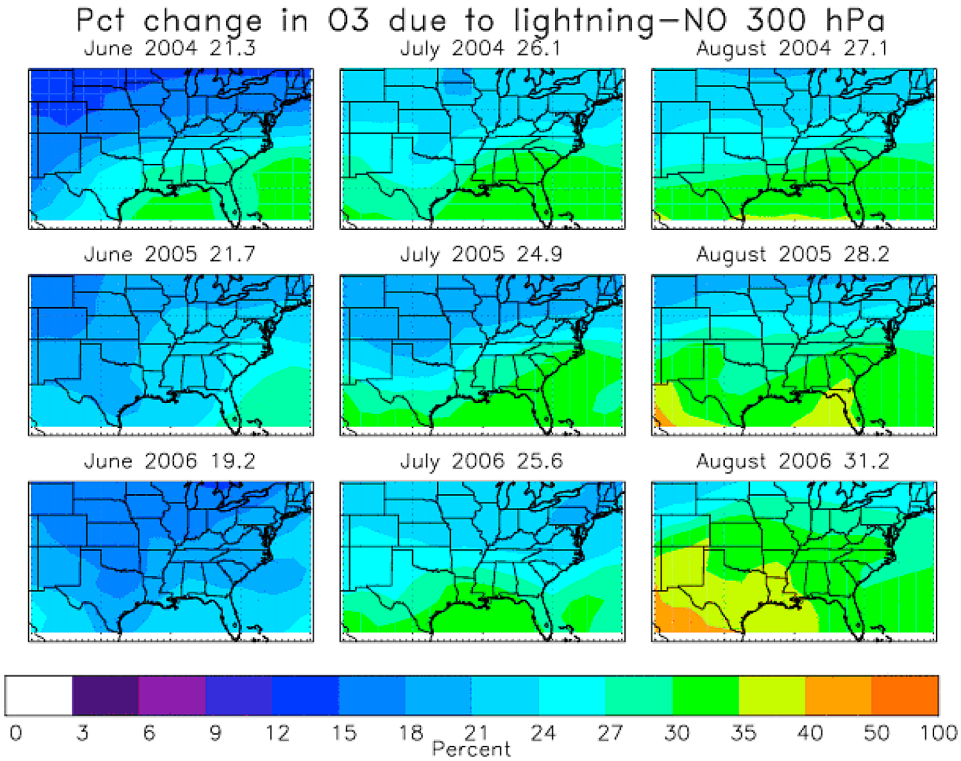

Figure 15. Percentage of 300 hPa ozone due to lightning NO emissions during (top) June, July, and August 2004, (middle) June, July, and August 2005, and (bottom) June, July, and August 2006. Results shown obtained by dividing differences between simulations high NO_x and No Lightning by results from simulation high NO_x.

lightning-produced NO resulting in an increase in ozone production from lightning NO emissions.

4. Impact of Lightning NO Emissions on Tropospheric Photochemistry

[51] Figures 12 and 13 show upper tropospheric (300 hPa) mixing ratios of NO_x and O_3 from GMI simulation high NO_x during summer 2004 (top), summer 2005 (middle), and summer 2006 (bottom). NO_x mixing ratios for simulation low NO_x are about 40% lower in the upper troposphere. Upper tropospheric ozone mixing ratios in simulation low NO_x are 7%–10% lower. Model upper tropospheric NO_x in the southeastern United States (100°W–70°W, 25°N–40°N) is largest during 2004 and smallest during 2006. However, model upper tropospheric ozone is smaller in 2004 than in 2006. The decrease in NO_x between 2004 and 2006 is sizable. Mean NO_x mixing ratios in 2004 average 0.23 ppbv while mean mixing ratios in 2006 average 0.15 ppbv. Increases in ozone are smaller in terms of percent. Mean 300 hPa ozone in summer 2004 averages 72.7 ppbv, while mean values in 2006 average 78.6 ppbv.

[52] The mean enhancement of 300 hPa NO_x resulting from lightning NO emissions was 67.5% (0.12 ppbv) (Figure 14). The contribution of lightning NO to 300 hPa NO_x is largest in 2004 and does not show a clear trend from June to August. Percentage contributions during these 9 months range from 61% to 73% at 300 hPa and vary little with pressure between 175 hPa (57%–68% contribution) and 400 hPa (61%–75% contribution). These percentage contributions agree closely with the results of *Zhao et al.* [2009] for 1 July 1 to 15 August 2004 (INTEX-A) but are a bit lower than those found by *Zhang et al.* [2003] for July in a MOZART-2 simulation driven by meteorological fields from a GCM. *Zhao et al.* [2009] found that lightning NO emissions contributed 60%–75% of 8–12 km NO_x over the INTEX-A region during the INTEX-A time period. *Zhang et al.* [2003] found that the lightning NO contribution to NO_x in the 5–15 km layer exceeded 90% for 30°N–40°N over the United States.

[53] The mean enhancement of 300 hPa ozone resulting from lightning NO emissions was 25.4% (17.4 ppbv) for simulation high NO_x (Figure 15). The contribution was smallest during June 2006 (19.2%), largest during August 2006 (31.2%), and varied only slightly with pressure between 175 (19%–30% contribution) and 500 hPa (18%–31% contribution). In contrast to NO_x, the contribution of lightning NO to upper tropospheric ozone increased from June to August. In units of ppbv, area-averaged monthly contributions from lightning in the GMI model ranged from 15 to 24 ppbv.

[54] Tables 3 and 4 summarize the methods used and results of other studies that have investigated the impact of lightning NO emissions on upper tropospheric photochemistry over North America. With few exceptions, the studies show that 60%–90% of upper tropospheric NO_x and 15%–35% of upper tropospheric ozone has a lightning NO source. This consensus exists despite the use of six different models and at least four different lightning parameterization schemes.

Table 3. Summary of Methods Used to Evaluate the Contribution of Summertime Lightning NO Emissions to Upper Tropospheric NO_x and Ozone Over the United States

Reference	Model Used	Time Period	Lightning Algorithm	IC/CG	IC:CG Energy	Vertical Partitioning	NO/Flash[a] INTEX Lightning Source[b]
Allen et al. [2010]	GMI	Jun–Aug 2004/2006	*Allen et al.* [2010]	N/A	1:1	*Ott et al.* [2010]	240 and 480 0.17 and 0.34
Bousserez et al. [2007]	MOCAGE	Jul–Aug 2004	*Price and Rind* [1992]	*Price and Rind* [1993]	1:10	*Mari et al.* [2006]	1100 for CG
Choi et al. [2008, 2009]	REAM	May–Aug 2005	*Choi et al.* [2005]	*Price and Rind* [1993]	1:1	*Pickering et al.* [1998]	300 N/A
Cooper et al. [2006]	FLEXPART	Jun–Aug 2004	NLDN/LRLDN[c]	*Boccippio et al.* [2001]	1:1	Gaussian between 6 km and tropopause	457 N/A
Cooper et al. [2007]	ECHAM5/MESSy	Aug 2006	*Price and Rind* [1992]	*Price and Rind* [1993]	1:10	*Pickering et al.* [1998]	6.6 Tg N/yr N/A
Cooper et al. [2009]	FLEXPART	Jun–Aug 2004/2006	NLDN/LRLDN[3]	*Boccippio et al.* [2001]	1:1	Gaussian 6km-tropopause	250 N/A
Fang et al. [2010]	MOZART-4	Jun–Aug 2004	*Price and Rind* [1992]	*Price and Rind* [1993]	1:10	Modified *Pickering* [1998]	800 for CG 0.27
Hudman et al. [2007, 2009]	GEOS-CHEM	Jul–Aug 2004	*Price and Rind* [1992]	N/A	1:1	*Pickering et al.* [1998]	125 and 500 0.07 and 0.27
Jourdain et al. [2009]	GEOS-CHEM	Jul 2006	*Price and Rind* [1992] scaled to OTDLIS/NLDN	N/A	1:1	*Pickering et al.* [1998]	260 and 520 0.10 and 0.28
Pfister et al. [2008]	MOZART-4	Jul–Aug 2004	*Price and Rind* [1992]	N/A	1:1	Modified *Pickering et al.* [1998]	5.6 Tg N/yr 0.06
Pierce et al. [2007]	RAQMS	Jul–Aug 2004	*Price and Rind* [1992]	*Price and Rind* [1993]	1:10	*Pickering et al.* [1998]	1100 for CG 0.16
Zhang et al. [2003]	MOZART-2	Jul	NLDN over U. S. *Price and Rind* [1992] elsewhere	*Boccippio* [2001] U. S. P&R (93) elsewhere	1:10	Uniform with height	7.0 Tg N/yr N/A
Zhao et al. [2009]	REAM	Jul–Aug 2004	*Choi et al.* [2005] but constrained by NLDN	*Price and Rind* [1993]	1:1	*Pickering et al.* [1998]	250 N/A

[a]Moles of NO per flash or if not available global source in Tg N/yr.
[b]Tg N emitted over the contiguous U. S. during the INTEX-A period.
[c]LRLDN (Long-Range Lightning Detection Network) [*Pessi et al.*, 2009].

[55] In summary, with the exception of the FLEXPART simulations that constrain flash rates using NLDN/LRLDN data, most models underestimated upper tropospheric NO_x amounts during INTEX-A by a factor of 2–3. Despite this underestimation, upper tropospheric ozone amounts were reasonably well simulated with most models having biases of less than 20%. For example, *Pfister et al.* [2008] show a 9–14 ppbv high bias between 9 and 12 km, while *Hudman et al.* [2007] show a 5–10 ppbv low bias for the same altitudes. These surprising results may be partially explained by the fact that DC-8 samples appear to be biased toward fresh convection [*Bertram et al.*, 2007], but they also suggest that future studies and/or field campaigns are needed to reduce uncertainties in stratosphere-troposphere exchange of ozone, ozone production rates, lightning NO emission rates, and upper tropospheric NO_x lifetimes. For example, samples of trace gas concentrations could be made within anvils and also 24–48 h later downwind of storms. These measurements could be coupled with three dimensional observations of flash rates to increase our understanding of the upper tropospheric budgets of NO_x and ozone.

5. Summary

[56] As part of an evaluation of the effect of clouds, convection, and lightning on tropospheric photochemistry, we have developed a new lightning parameterization scheme for the GMI model and used it to simulate the 2004–2006 time period and to evaluate the summertime contribution of lightning NO emissions to upper tropospheric NO_x and ozone over the eastern United States and the adjacent Atlantic Ocean.

[57] This parameterization replaces the default scheme in which lightning NO emissions were a function of climatological monthly average ISCCP cloud top heights [*Price et al.*, 1997]. The new scheme is similar to the scheme of *Allen and Pickering* [2002] in that it uses upward cloud mass flux in the upper troposphere as the indicator of when and where lightning NO emissions occur. The 2002 scheme used upward cloud mass flux as the predictor variable for lightning flash rate through best fit polynomials developed from ranked distributions of this variable and observed NLDN flash rates. The new scheme assumes flash rates are proportional to the square of upward convective mass flux but then adjusts flash rates locally and monthly so that flash rates when averaged over a time period of interest best match v2.2 of the OTD/LIS climatology for each grid box and month. Overall, the spatial distribution of observed flashes is reasonably well captured by the mass flux square based parameterization. Both observed and model flash rates are largest in a band that extends from southern Louisiana to central Florida although model flash rates are often 20%–40% too low in this region when compared with adjusted NLDN data. Month-to-month variations in flash rate location are also well captured by the model.

[58] In agreement with several other studies, we find that upper tropospheric model NO_x is much lower than measured NO_x during the INTEX-A field campaign. Middle tropospheric (7–9 km) biases for high NO_x simulations range from a factor of 1.2–1.7 depending on the vertical partitioning of lightning NO emissions while upper tropospheric (9–12 km) biases range from 2.2 to 3.6.

Table 4. Overview of Results From Studies That Evaluated the Contribution of Lightning NO Emissions to Upper Tropospheric NO_x and Ozone Over the United States

Reference	Upper Tropospheric NO_x Bias During INTEX-A	Impact of Lightning NO on NO_x	Impact of Lightning NO on Ozone
Allen et al. [2010]	Median is factor of 1.7 (3.6) too low for 7–9 (9–12 km)	57%–75% of upper tropospheric NO_x has lightning source	18%–31% (15–24 ppbv) of upper tropospheric ozone has lightning source
Bousserez et al. [2007]	Median is a factor of 1.3 (2.3) too low for 7–9 (9–12 km)	Lightning NO is responsible for upper tropospheric peak in NO_x	N/A
Choi et al. [2008, 2009]	N/A	Tropospheric NO_2 column enhancement over United States by lightning is 40%–60% of enhancement due to anthropogenic emissions	Tropospheric O_3 column enhanced by 15%–22%; 8–20+ ppbv increases in upper tropospheric O_3 in southern United States
Cooper et al. [2006]	N/A	78%–95% of 6–12 km NO_x over southeastern United States has lightning source	North American lightning NO contributes 69%–84% (11–13 ppbv) of summer 2004 enhancement in upper tropospheric eastern U. S. O_3 with respect to western United States
Cooper et al. [2007]	N/A	N/A	25–30 ppbv increase in upper tropospheric ozone over southern United States during August 2006
Cooper et al. [2009]	Mean shows high bias of 50% (70%) for 6–9 (9–12) km; median shows 0% (30%) low bias for 6–9 (9–12) km	More than 80% of upper tropospheric NO_x over eastern and southern United States has a lightning NO source	N/A
Fang et al. [2010]	Mean for high-NO_x simulation is a factor of 1.6 (2.4) too low for 8–10 (10–12) km	Responsible for 24%–43% of free troposphere NO_y export from the United States and 28–34% of NO_y wet deposition	Increases ozone production in Northern Hemisphere extratropics by 33% and reduces ozone production efficiency in free troposphere by 30%
Hudman et al. [2007, 2009]	Median is factor of 1.5–2.5 too low for high-NO_x simulation	N/A	Lightning NO increases hemispheric tropospheric O_3 burden by 5%–6% with 10–17 ppbv upper tropospheric enhancement over southeastern United States
Jourdain et al. [2009]	N/A	N/A	Increasing midlatitude lightning NO source decreased 300 hPa biases wrt TES and IONS
Pfister et al. [2008]	Mean shows low bias of 150 (500) pptv for 8–10 (10–12) km	N/A	10–20 ppbv (15%–30%) enhancement of upper tropospheric ozone over United States due to lightning NO
Pierce et al. [2007]	Median NO_2 is a factor of 2 too low at 300 hPa	N/A	Lightning NO is large contributor to upper tropospheric ozone export from the United States
Zhang et al. [2003]	N/A	Lightning NO contribution to upper tropospheric NO_x exceeds 90% for 30°N–40°N	20%–35% increase for 5–12 km
Zhao et al. [2009]	Unbiased south of 35°N; factor of 2–4 too low north of 35°N	60%–75% of upper tropospheric NO_x has lightning source	Upper tropospheric enhancements of 10–20 ppbv

[59] Biases between modeled and satellite-retrieved tropospheric NO_2 columns are also sensitive to the lightning NO source. Tropospheric NO_2 columns from the OMI DP-GC product and the GMI model were compared over the eastern United States during the summers of 2005 and 2006. Over the northeastern United States, GMI columns exceeded DP-GC columns by 3% (18%) for the low NO_x (high NO_x) simulation. Comparison of model NO emissions with CEMS measurements indicates that much of the overestimation is due to an overestimation of anthropogenic emissions over the Ohio River Valley during this period. Over the southeastern United States, GMI columns were 13% lower than DP-GC columns in the low NO_x simulation and 7% higher than the DP-GC columns in the high NO_x simulation.

[60] Upper tropospheric ozone amounts agreed reasonably well with measurements despite the upper tropospheric low bias in NO_x. Mean model 316 hPa ozone amounts showed a 7 (2) ppbv low bias with respect to TES for the low NO_x (high NO_x) simulation. Mean model 7–12 km ozone showed a -9 ± 5 (1 ± 5) ppbv bias with respect to eastern U. S. IONS ozonesondes for the low NO_x (high NO_x) simulation. Mean model 7–12 km ozone did show a high bias with respect to INTEX-A measurements. The bias ranged from 4 ± 7 ppbv for the low NO_x simulation to 14 ± 9 ppbv for the high NO_x simulation.

[61] Overall, comparisons with upper tropospheric INTEX-A NO_x measurements, OMI DP-GC tropospheric NO_2 columns, TES ozone retrievals, and upper tropospheric IONS ozone profiles argue that the high NO_x simulation that includes a 480 mol per flash NO source is the most realistic. This high NO_x source reduces low biases with respect to INTEX-A NO_x, TES ozone, and IONS ozone, while introducing a small high bias with respect to the OMI DP-GC product. This high bias is not a major concern given the uncertainties in and between tropospheric NO_2 products and the uncertainties introduced by the use of averaging kernels. Possible causes of the remaining upper tropospheric low bias with respect to the INTEX-A NO_x measurements include a mistiming or misplacement of deep convection, an underestimation of its vertical extent and/or too rapid NO_x chemistry in the upper troposphere in the model.

[62] Lightning NO emissions are an important contributor to the ozone profiles at southeastern U. S. IONS sites with the mean upper tropospheric (7–12 km) summertime enhancement of ozone associated with lightning NO for simulation high NO_x equaling 21 ppbv in 2004 and 30 ppbv in 2006. Observed changes in upper tropospheric ozone at southeastern U. S. IONS sites between 2004 and 2006 (−6 to +11 ppbv) are captured by the GMI model when it includes a lightning NO source. These changes appear to be caused by 5–13 ppbv increases between 2004 and 2006 in the amount of ozone originating from lightning NO emissions. These increases occur despite the fact that model lightning NO emissions are 15%–20% larger in 2004 than 2006. A stronger upper tropospheric anticyclone in 2006 than in 2004 led to longer NO lifetimes and additional ozone formation.

[63] Finally, we looked at the contribution of lightning NO emissions to upper tropospheric NO_x and ozone amounts. For the high NO_x simulation, the contribution of lightning NO to 300 hPa NO_x (ozone) during summer months varied from 61% to 73% (19%–31%) with the contribution to ozone but not NO_x increasing as the summer progressed. Percent contributions did not vary much with altitude within the upper troposphere.

Appendix A: Application of DOMINO Averaging Kernel to GMI Product

[64] Whenever the GMI model is run, gridded "overpass" files are produced each day containing selected variables at the time of Aura satellite overpasses. For comparison with the DOMINO product, NO_2 mixing ratios were extracted from the 13:30 local time overpass file. These NO_2 mixing ratios were interpolated onto the vertical grid of the TM4 CTM, the CTM that was used to provide first-guess columns for the DOMINO product [*Boersma et al.*, 2007]. NO_2 partial columns (X) were then calculated for each TM4 layer from the GMI output. In order to ensure mass conservation, the surface pressure from the GMI model as opposed to the TMI model was used when calculating the partial column of the lowest layer. Finally, the tropospheric raw (unprocessed) NO_2 column ($\mathrm{Yraw}_{\mathrm{trop}}$) was obtained by summing X within the troposphere.

[65] In many instances, it makes sense to apply an averaging kernel to the model output before comparing with satellite-retrieved fields. The "averaging-kernel processed" tropospheric NO_2 column (Y_{trop}) is calculated by taking the dot product of X within the troposphere (X_{trop}) and the tropospheric averaging kernel, where the tropospheric averaging kernel is obtained by multiplying the averaging kernel (A) by $\mathrm{AMF}/\mathrm{AMF}_{\mathrm{trop}}$, where $\mathrm{AMF}/\mathrm{AMF}_{\mathrm{trop}}$ is the ratio of the total air mass factor to the tropospheric air mass factor. Mathematically,

$$Y_{\mathrm{trop}} = X_{\mathrm{trop}} \times A \times \mathrm{AMF}/\mathrm{AMF}_{\mathrm{trop}}. \tag{A1}$$

The A, the number of tropospheric layers "TM4TropoPause-Level," and the air mass factors are available within the level 2 DOMINO product.

[66] For comparison with $\mathrm{Yraw}_{\mathrm{trop}}$ and Y_{trop}, the level 2 DOMINO fields were mapped onto the GMI grid. The mapping of the DOMINO product was done in three steps. In step 1, retrievals contaminated by clouds were removed from the DOMINO data sets. This step involved removing level 2 DOMINO pixels with a radiative cloud fraction exceeding 0.5 or a snowy/icy surface [*Boersma et al.*, 2007]. This threshold ends up removing approximately 50% of the pixels. On 30 June 2006, for example, the 0.5 radiative threshold removed 56% of OMI DOMINO pixels. The threshold is somewhat arbitrary and monthly average tropospheric NO_2 columns are sensitive to the cloud screening thresholds with mean columns generally increasing as the threshold is decreased. In step 2, daily gridded tropospheric NO_2 columns were created by averaging level 2 NO_2 columns within each $2° \times 2.5°$ GMI grid box. A missing data flag was used at grid boxes that did not have a valid OMI sample that day. In step 3, monthly average tropospheric NO_2 columns were created by averaging the valid daily average values.

[67] **Acknowledgments.** This work was funded by the NASA Modeling, Analysis, and Prediction Program under NASA grant NNG06GE01G, "Effects of clouds, convection, and lightning on tropo-

spheric chemistry in the GMI model." We thank Anne Thompson for access to the IONS ozonesonde data, Dylan Jones for guidance in applying TES averaging kernels, K. F. Boersma for guidance in the use of DOMINO NO_2 fields, and L. Lamsal for access to the DP-GC NO_2 data. OTD/LIS data are from NASA/MSFC. NLDN data are collected by Vaisala Inc. and are archived at NASA-MSFC.

References

Allen, D. J., and K. E. Pickering (2002), Evaluation of lightning flash rate parameterizations for use in a global chemical transport model, *J. Geophys. Res.*, *107*(D23), 4711, doi:10.1029/2002JD002066.

Atkinson, R., and J. Arey (2003), Gas-phase tropospheric chemistry of biogenic volatile compounds: a review, *Atmos. Environ.*, *37*, S197–S219.

Berntsen, T. K., and I. S. A. Isaksen (1999), Effects of lightning and convection on changes in tropospheric ozone due to NO_x emissions from aircraft, *Tellus*, *51B*, 766–788.

Bertram, T. H., et al. (2007), Direct measurements of the convective recycling of the upper troposphere, *Science*, *315*, 816–820, doi:10.1126/science.1134548.

Bey, I., B. Aumont, and G. Toupance (2001), A modeling study of the nighttime radical chemistry in the lower continental troposphere: 1. Development of a detailed chemical mechanism including nighttime chemistry, *J. Geophys. Res.*, *106*(D9), 9959–9990, doi:10.1029/2000JD900347.

Biagi, C. J., K. L. Cummins, K. E. Kehoe, and E. P. Krider (2007), National Lightning Detection Network (NLDN) performance in southern Arizona, Texas, and Oklahoma in 2003–2004, *J. Geophys. Res.*, *112*, D05208, doi:10.1029/2006JD007341.

Bian, H., and M. J. Prather (2002), Fast-J2: Accurate Simulation of stratospheric photolysis in global chemical models, *J. Atmos. Chem.*, *41*, 281–296.

Biazar, A. P., and R. T. McNider (1995), Regional estimates of lightning production of nitrogen oxides, *J. Geophys. Res.*, *100*(D11), 22,861–22,874, doi:10.1029/95JD01735.

Bloom, S., et al. (2005), Documentation and validation of the Goddard Earth Observing System (GEOS) data assimilation system, version 4, *NASA Tech. Rep. Ser.* Global Modeling Data Assimilation, NASA/TM 104606, vol. *26*.

Bloomer, B. J., J. W. Stehr, C. A. Piety, R. J. Salawitch, and R. R. Dickerson (2009), Observed relationships of ozone air pollution with temperature and emissions, *Geophys. Res. Lett.*, *36*, L09803, doi:10.1029/2009GL037308.

Boccippio, D., K. Driscoll, W. Koshak, R. Blakeslee, W. Boeck, D. Mach, D. Buechler, H. J. Christian, and S. J. Goodman (2000), The Optical Transient Detector (OTD): Instrument characteristics and cross-sensor validation, *J. Atmos. Oceanic Technol.*, *17*, 441–458.

Boccippio, D., K. Cummins, H. Christian, and S. Goodman (2001), Combined satellite- and surface-based estimation of the intracloud-cloud-to-ground lightning ratio over the continental United States, *Mon. Weather. Rev.*, *129*, 108–122.

Boccippio, D. J., W. J. Koshak, and R. J. Blakeslee (2002), Performance assessment of the optical transient detector and lightning imaging sensor: I. Predicted diurnal variability, *J. Atmos. Oceanic Technol.*, *19*, 1318–1332. Boersma, K. F., et al. (2007), Near real-time retrieval of tropospheric NO_2 from OMI, *Atmos. Chem. Phys.*, *112*, 2103–2118.

Bond, D. W., R. Zhang, X. Tie, G. Brasseur, G. Huffines, R. E. Orville, and D. J. Boccippio (2001), NO_x production by lightning over the continental United States, *J. Geophys. Res.*, *106*(D21), 27,701–27,710, doi:10.1029/2000JD000191.

Bond, D. W., S. Steiger, R. Zhang, X. Tie, and R. E. Orville (2002), The importance of NO_x production by lightning in the tropics, *Atmos. Environ.*, *36*, 1509–1519.

Bousserez, N. et al. (2007), Evaluation of the MOCAGE chemistry transport model during the ICARTT/ITOP experiment, *J. Geophys. Res.*, *112*, D10S42, doi:10.1029/2006JD007595.

Bucsela, E. J., et al. (2008), Comparison of tropospheric NO_2 from in situ aircraft measurements with near-real-time and standard product data from OMI, *J. Geophys. Res.*, *113*, D16S31, doi:10.1029/2007JD008838.

Celarier, E. A., et al. (2008), Validation of ozone monitoring instrument nitrogen dioxide columns, *J. Geophys. Res.*, *113*, D15S15, doi:10.1029/2007JD008908.

Chin, M., P. Ginoux, S. Kinne, O. Torres, B. N. Holben, B. N. Duncan, R. V. Martin, J. A. Logan, A. Higurashi, and T. Nakajimaet (2002), Tropospheric aerosol optical thickness from the GOCART model and comparisons with satellite and sunphotometer measurements, *J. Atmos. Sci.*, *59*, 461–483.

Choi, Y., Y. Wang, T. Zeng, R. V. Martin, T. P. Kurosu, and K. Chance (2005), Evidence of lightning NO_x and convective transport of pollutants in satellite observations over North America, *Geophys. Res. Lett.*, *32*, L02805, doi:10.1029/2004GL021436.

Choi, Y., Y. Wang, Q. Yang, D. Cunnold, T. Zeng, C. Shim, M. Luo, A. Eldering, E. Bucsela, and J. Gleason (2008), Spring to summer northward migration of high O_3 over the western North Atlantic, *Geophys. Res. Lett.*, *35*, L04818, doi:10.1029/2007GL032276.

Choi, Y., J. Kim, A. Eldering, G. Osterman, Y. L. Yung, Y. Gu, and K. N. Liou (2009), Lightning and anthropogenic NO_x sources over the United States and the western North Atlantic Ocean: Impact on OLR and radiative effects, *Geophys. Res. Lett.*, *36*, L17806, doi:10.1029/2009GL039381.

Christian, H. J., et al. (2003), Global frequency and distribution of lightning as observed from space by the optical transient detector, *J. Geophys. Res.*, *108*(D1), 4005, doi:10.1029/2002JD002347.

Considine, D. B., J. A. Logan, and M. A. Olsen (2008), Evaluation of near-tropopause ozone distributions in the global modeling initiative combined stratosphere/troposphere model with ozonesonde data, *Atmos. Chem. Phys.*, *8*, 2364–2385.

Cooper, O. R., et al. (2006), Large upper tropospheric ozone enhancements above midlatitude North America during summer: In situ evidence from the IONS and MOZAIC ozone measurement network, *J. Geophys. Res.*, *111*, D24S05, doi:10.1029/2006JD007306.

Cooper, O. R., et al. (2007). Evidence for a recurring eastern North American upper tropospheric ozone maximum during summer, *J. Geophys. Res.*, *112*, D23304, doi:10.1029/2007JD008710.

Cooper, O. R., et al. (2009), Summertime buildup and decay of lightning NO and aged thunderstorm outflow above North America, *J. Geophys. Res.*, *114*, D01101, doi:10.1029/2008JD010293.

Cooray, V., M. Rahman, and V. Rakov (2009), On the NO_x production by laboratory electrical discharges and lightning, *J. Atmos. Sol. Terr. Phys.*, *71*, 1877–1889, doi:10.1016/j.jastp.2009.07.009.

Cummins, K., M. Murphy, E. Bardo, W. Hiscox, R. Pyle, and A. Pifer (1998), A combined TOA/MDF technology upgrade of the U. S. National Lightning Detection Network, *J. Geophys. Res.*, *103*(D8), 9035–9044, doi:10.1029/98JD00153.

DeCaria, A., K. Pickering, G. Stenchikov, J. Scala, J. Stith, J. Dye, B. Ridley, and P. Laroche (2000), A cloud-scale model study of lightning-generated NO_x in an individual thunderstorm during STERAO-A, *J. Geophys. Res.*, *105*(D9), 11,601–11,616.

DeCaria, A. J., K. E. Pickering, G. L. Stenchikov, and L. E. Ott (2005), Lightning-generated NO_x and its impact on tropospheric ozone production: A three-dimensional modeling study of a STERAO-A thunderstorm, *J. Geophys. Res.*, *110*, D14303, doi:10.1029/2004JD005556.

Duncan, B. N., S. E. Strahan, Y. Yoshida, S. D. Steenrod, and N. Livesey (2007), Model study of the cross-tropopause transport of biomass burning pollution, *Atmos. Chem. Phys.*, *7*, 3713–3736.

Duncan, B. N., J. J. West, Y. Yoshida, A. M. Fiore, and J. R. Ziemke (2008), The influence of European pollution on ozone in the Near East and northern Africa, *Atmos. Chem. Phys.*, *8*, 2267–2283.

Dunlea, E. J., and A. R. Ravishankara (2004), Kinetic studies of the reactions of O(1D) with several atmospheric molecules, *Phys. Chem.*, doi:10.1039/b400247d.

Evans, M. J., and D. J. Jacob (2005), Impact of new laboratory studies of NO hydrolysis on global model budgets of tropospheric nitrogen oxides, ozone, and OH, *Geophys. Res. Lett.*, *32*, L09813, doi:10.1029/2005GL022469.

Fang, Y., A. M. Fiore, L. W. Horowitz, H. Levy II, Y. Hu, and A. G. Russell (2010), Sensitivity of the NO_y budget over the United States to anthropogenic and lightning NO_x in summer, *J. Geophys. Res.*, *115*, D18312, doi:10.1029/2010JD014079.

Fehr, T., H. Höller, and H. Huntrieser (2004), Model study on production and transport of lightning-produced NO_x in a EULINOX supercell storm, *J. Geophys. Res.*, *109*, D09102, doi:10.1029/2003JD003935.

Frost, G. J., et al. (2006), Effects of changing power plant NO_x emissions on ozone in the eastern United States: Proof of concept, *J. Geophys. Res.*, *111*, D12306, doi:10.1029/2005JD006354.

Grewe, V. (2007), Impact of climate variability on tropospheric ozone, *Sci. Total Environ.*, *374*, 167–181, doi:10.1016/j.scitotenv.2007.01.032.

Grewe, V., D. Brunner, M. Dameris, J. L. Grenfell, R. Hein, D. Shindell, and J. Staehelin (2001), Origin and variability of upper tropospheric nitrogen oxides and ozone at northern midlatitudes, *Atmos. Environ.*, *35*, 3421–3433.

Guenther, A., T. Karl, P. Harley, C. Wiedinmyer, P. I. Palmer, and C. Geron (2006), Estimates of global terrestrial isoprene emissions using MEGAN (Model of Emissions of Gases and Aerosols from Nature), *Atmos. Chem. Phys.*, *6*, 3181–3210.

Hauglustaine, D., L. Emmons, M. Newchurch, G. Brasseur, T. Takao, K. Matsubara, J. Johnson, B. Ridley, J. Stith, and J. Dye (2001), On

the role of lightning NO_x in the formation of tropospheric ozone plumes: A global model perspective, *J. Atmos. Chem.*, *38*, 277–294.

Henderson, B., et al. (2010), Evaluation of simulated photochemical partitioning of oxidized nitrogen in the upper troposphere, *Atmos. Chem. Phys. Discuss.*, *10*, 20,125–20,165, doi:10.5194/acpd-10-20125-2010.

Hudman, R. C., et al. (2007), Surface and lightning sources of nitrogen oxides over the United States: Magnitudes, chemical evolution, and outflow, *J. Geophys. Res.*, *112*, D12S05, doi:10.1029/2006JD007912.

Hudman, R. C., L. T. Murray, D. J. Jacob, S. Turquety, S. Wu, D. B. Millet, M. Avery, A. H. Goldstein, and J. Holloway (2009), North American influence on tropospheric ozone and the effects of recent emission reductions: Constraints from ICARTT observations, *J. Geophys. Res.*, *114*, D07302, doi:10.1029/2008JD010126.

Huntrieser, H., U. Schumann, H. Schlager, H. Höller, A. Giez, H.-D. Betz, D. Brunner, C. Forster, O. Pinto Jr., and R. Calheiros (2008), Lightning activity in Brazilian thunderstorms during TROCCINOX: Implications for NO_x production, *Atmos. Chem. Phys.*, *8*, 21–953.

Jacobson, M. Z. (1995), Computation of global photochemistry with SMVGEAR II, *Atmos. Environ.*, *29A*, 2541–2546.

Jöckel, et al. (2006), The atmospheric chemistry general circulation model ECHAM5/MESSy, Consistent simulation of ozone from the surface to the mesosphere, *Atmos. Chem. Phys.6*, 5067–5104.

Jourdain, L., S. S. Kulawik, H. M. Worden, K. E. Pickering, J. Worden, and A. M. Thompson (2010), Lightning NO_x emissions over the USA constrained by TES ozone observations and the GEOS-Chem model, *Atmos. Chem. Phys.*, *10*, 107–119.

Kiehl, J. T., J. J. Hack, G. B. Bonan, B. A. Boville, B. P. Briegleb, D. L. Williamson, and P. J. Rasch (1985), Description of the NCAR Community Climate Model (CCM3), *Tech. Rep.*, *NCAR/TN-420+STR*, NCAR, Boulder, CO.

Kiehl, J. T., J. J. Hack, G. B. Bonan, B. A. Boville, D. L. Williamson, and P. J. Rasch (1998), The National Center for Atmospheric Research Community Climate Model: CCM, *J. Clim.*, *11*, 1131–1150.

Kim, W., et al. (2009), NO columns in the western United States observed from space and simulated by a regional chemistry model and their implications for NO emissions, *J. Geophys. Res.*, *114*, D11301, doi:10.1029/2008JD011343.

Lamarque, J. F., G. P. Brasseur, P. G. Hess, and J. F. Mueller (1996), Three-dimensional study of the relative contributions of the different nitrogen sources in the troposphere, *J. Geophys. Res.*, *101*(D17), 22,955–22,968, doi:10.1029/96JD02160.

Lamsal, L. N., R. V. Martin, A. van Donkelaar, E. A. Celarier, E. J. Bucsela, K. F. Boersma, R. Dirksen, C. Luo, and Y. Wang (2010), Indirect validation of tropospheric nitrogen dioxide retrieved from the OMI satellite instrument: Insight into the seasonal variation of nitrogen oxides at northern midlatitudes, *J. Geophys. Res.*, *115*, D05302, doi:10.1029/2009JD013351.

Levy, H., II, W. J. Moxim, A. A. Klonecki, and P. S. Kasibhatla (1999), Simulated tropospheric NO_x: its evaluation, global distribution, and individual source contributions, *J. Geophys. Res.*, *104*(D21), 26,279–26,306, doi:10.1029/1999JD900442.

Li, Q., D. J. Jacob, R. Park, Y. Wang, C. L. Heald, R. Hudman, R. M. Yantosca, R. V. Martin, and M. Evans (2005), North American pollution outflow and the trapping of convectively lifted pollution by upper-level anticyclone, *J. Geophys. Res.*, *110*, D10301, doi:10.1029/2004JD005039.

Lin, S. J. (2004), A "vertically Lagrangian" finite-volume dynamical core for global models, *Mon. Weather. Rev.*, *124*, 2046–2070.

Mach, D. M., H. J. Christian, R. J. Blakeslee, D. J. Boccippio, S. J. Goodman, and W. L. Boeck (2007), Performance assessment of the optical transient detector and lightning imaging sensor, *J. Geophys. Res.*, *112*, D09210, doi:10.1029/2006JD007787.

Mari, C., J. P. Chaboureau, J. P. Pinty, J. Duron, P. Mascart, J. P. Camas, and F. Gheusi (2006), Regional lightning NO_x sources during the TROCCINOX experiment, *Atmos. Chem. Phys.*, *6*, 5559–5572.

Martin, R. V., et al. (2003), Global and regional decreases in tropospheric oxidants from photochemical effects of aerosols, *J. Geophys. Res.*, *108* (D3), 4097, doi:10.1029/2002JD002622.

Martin, R. V., et al. (2006), Evaluation of space-based constraints on global nitrogen oxide emissions with regional aircraft measurements over and downwind of eastern North America, *J. Geophys. Res.*, *111*, D15308, doi:10.1029/2005JD006680.

Nassar, R., et al. (2008), Validation of Tropospheric Emission Spectrometer (TES) nadir ozone profiles using ozonesonde measurements, *J. Geophys. Res.*, *113*, D15S17, doi:10.1029/2007JD008819.

Orville, R. E., and G. R. Huffines (2001), Cloud-to-ground lightning in the United States: NLDN results in the first decade, 1989–1998, *Mon. Weather. Rev.*, *129*, 1179–1193.

Osterman, G., et al. (2009), Earth Observing System (EOS), Tropospheric Emission Spectrometer (TES), Level 2 (L2), Data User's Guide, D-38042, version 4.0. (Available at http://eosweb.larc.nasa.gov/PRODOCS/tes/UsersGuide/TES_L2_Data_Users_Guide.pdf.)

Ott, L. E., K. E. Pickering, G. L. Stenchikov, H. Huntrieser, and U. Schumann (2007), Effects of lightning NO_x production during the 21 July European Lightning Nitrogen Oxides Project storm studied with a three-dimensional cloud-scale chemical transport model, *J. Geophys. Res.*, *112*, D05307, doi:10.1029/2006JD007365.

Ott, L. E., K. E. Pickering, G. L. Stenchikov, D. J. Allen, A. J. DeCaria, B. Ridley, R.-F. Lin, S. Lang, and W.-K. Tao (2010), Production of lightning NO_x and its vertical distribution calculated from three-dimensional cloud-scale chemical transport model simulations, *J. Geophys. Res.*, *115*, D04301,doi:10.1029/2009JD011880.

Pawson, S., R. S. Stolarski, A. R. Douglass, P. A. Newman, J. E. Nielsen, S. M. Frith, and M. L. Gupta (2008), Goddard Earth Observing System chemistry-climate model simulations of stratospheric ozone-temperature coupling between 1950 and 2005, *J. Geophys. Res.*, *113*, D12103, doi:10.1029/2007JD009511.

Pfister, G. G., L. K. Emmons, P. G. Hess, J.-F. Lamarque, A. M. Thompson, and J. E. Yorks (2008), Analysis of the Summer 2004 ozone budget over the United States using Intercontinental Transport Experiment Ozonesonde Network Study (IONS) observations and Model of Ozone and Related Tracers (MOZART-4) simulations, *J. Geophys. Res.*, *113*, D23306, doi:10.1029/2008JD010190.

Pessi, A. T., S. Businger, K. L. Cummins, N. W. S. Demetriades, M. Murphy, and B. Pifer (2009), Development of a Long-Range Lightning Detection Network for the Pacific: Construction, Calibration, and Performance, *J. Atmos. Oceanic Technol.*, *26*, 145–166.

Pickering, K., Y. Wang, W. K. Tao, C. Price, and J. F. Müller (1998), Vertical distributions of lightning NO_x for use in regional and global chemical transport models, *J. Geophys. Res.*, *103*(D23), 31,203–31,216, doi:10.1029/98JD02651.

Pierce, R. B., et al. (2007), Chemical data assimilation estimates of continental U. S. ozone and nitrogen budgets during the Intercontinental Chemical Transport Experiment-North America, *J. Geophys. Res.*, *112*, D12S21, doi:10.1029/2006JD007722.

Price, C., and D. Rind (1992), A simple lightning parameterization for calculating global lightning distributions, *J. Geophys. Res.*, *97*(D9), 9919–9933, doi:10.1029/92JD00719.

Price, C., and D. Rind (1993), What determines the cloud-to-ground lightning fraction in thunderstorms?, *Geophys. Res. Lett.*, *20*(6), 463–466, doi:10.1029/93GL00226.

Price, C., J. Penner, and M. Prather (1997), NO_x from lightning 1. Global distribution based on lightning physics, *J. Geophys. Res.*, *102*(D5), 5929–5941, doi:10.1029/96JD03504.

Ravishankara, A. R., E. J. Dunlea, M. A. Blitz, T. J. Dillon, D. E. Heard, M. J. Pilling, R. S. Strekowski, J. M. Nicovich, and P. H. Wine (2002), Redetermination of the rate coefficient for the reaction of $O(^1D)$ with N_2, *Geophys. Res. Lett.*, *29*(15), 1745, doi:10.1029/2002GL014850.

Ridley, B. A., K. E. Pickering, and J. E. Dye (2005), Comments on the parameterization of lightning-produced NO in global chemistry-transport models, *Atmos. Environ.*, *39*, 6184–6187.

Rienecker, M. M., et al. (2008), The GEOS-5 Data Assimilation System, Documentation of Versions 5.0.1, 5.1.0, and 5.2.0, *NASA Tech. Rep. Ser.*, Global Modeling and Data Assimilation, vol. *27*.

Rossow, W. B., A. W. Walker, D. E. Beuschel, and M. D. Roiter (1996), International Satellite Cloud Climatology Project (ISCCP) documentation of new cloud data sets, *WMO/TD 737*, 115 pp., World Meteorol. Org., Geneva.

Schumann, U., and H. Huntrieser (2007), The global lightning-induced nitrogen oxides source, *Atmos. Chem. Phys.*, *7*, 3823–3907.

Singh, H. B., W. H. Brune, J. H. Crawford, D. J. Jacob, and P. B. Russell (2006), Overview of the summer 2004 Intercontinental Chemical Transport Experiment-North America (INTEX-A), *J. Geophys. Res.*, *111*, D24S01, doi:10.1029/2006JD007905.

Singh, H. B., et al. (2007), Reactive nitrogen distribution and partitioning in the North American troposphere and lowermost stratosphere, *J. Geophys. Res.*, *112*, D12S04, doi:10.1029/2006JD007664.

Thompson, A. M., et al. (2007a), Intercontinental Chemical Transport Experiment Ozonesonde Network Study (IONS) 2004: 2. Tropospheric ozone budgets and variability over northeastern North America, *J. Geophys. Res.*, *112*, D12S13, doi:10.1029/2006JD007670.

Thompson, A. M., et al. (2007b), Intercontinental Chemical Transport Experiment Ozonesonde Network Study (IONS) 2004: 1. Summertime upper troposphere/lower stratosphere ozone over northeastern North America, *J. Geophys. Res.*, *112*, D12S12, doi:10.1029/2006JD007441.

Tie, X., R. Zhang, G. Brasseur, L. Emmons, and W. Lei, (2001), Effects of lightning on reactive nitrogen and nitrogen reservoir species in the tropo-

sphere, *J. Geophys. Res.*, *106*(D3), 3167–3178, doi:10.1029/2000JD900565.

Tyndall, G. S., R. A. Cox, C. Granier, R. Lesclaux, G. K. Moortgat, M. J. Pilling, A. R. Ravishankara, and T. J. Wallington (2001), Atmospheric chemistry of small organic peroxy radicals, *J. Geophys. Res.*, *106*(D11), 12,157–12,182, doi:10.1029/2000JD900746.

Van der Werf, G. R., J. T. Randerson, L. Giglio, G. J. Collatz, P. S. Kasibhatla, A. F. Arellano (2006), Interannual variability in global biomass burning emissions from 1997 to 2004, *Atmos. Chem. Phys.*, *6*, 3423–3441.

Wang, Y., and T. Zeng (2004), On tracer correlations in the troposphere: The case of ethane and propane, *J. Geophys. Res.*, *109*, D24306, doi:10.1029/2004JD005023.

Wild, O., X. Zhu, and M. Prather (2000), Fast-J: Accurate simulation of in- and below-cloud photolysis in tropospheric chemical models, *J. Atmos. Chem.*, *37*, 245–282.

Xiao, Y., D. J. Jacob, and S. Turquety (2007), Atmospheric acetylene and its relationship with CO as an indicator of air mass age, *J. Geophys. Res.*, *112*, D12305, doi:10.1029/2006JD008268.

Zhang, G. J., and N. A. McFarlane (1995), Sensitivity of climate simulations to the parameterization of cumulus convection in the Canadian Climate Centre general circulation model, *Atmos. Ocean.*, *33*, 407–446.

Zhang, R., X. Tie, and D. W. Bond (2003), Impacts of anthropogenic and natural NO_x sources over the U. S. on tropospheric chemistry, *Proc. Natl. Acad. Sci. U. S.A.*, *100*(4), 1505–1509, doi:10.1073/pnas.252763799.

Zhao, C., Y. Wang, Y. Choi, and T. Zeng (2009), Summertime impact of convective transport and lightning NO_x production over North America: modeling dependence on meteorological simulations, *Atmos. Chem. Phys.*, *9*, 4315–4327.

D. Allen, Department of Meteorology, University of Maryland College Park, College Park, MD 20742, USA. (allen@atmos.umd.edu)

M. Damon, Northrop Grumman Information Technology and Software Integration and Visualization Office (Code 610.3), NASA-GSFC, Greenbelt, MD 20771, USA.

B. Duncan and K. Pickering, NASA-GSFC, Code 613.3, Greenbelt, MD 20771, USA.